Rejuvenation-Responsive and Senolytic-Sensitive Muscle Stem Cells Unveiled by CD200 and CD63 in Geriatric Muscle

Ye Lynne Kim[1†], Young-Woo Jo[1†], Takwon Yoo[1†], Kyusang Yoo[1], Ji-Hoon Kim[2], Myungsun Park[3], In-Wook Song[1], Hyun Kim[1], Yea-Eun Kim[1], Sang-Hyeon Hann[1], Jong-Eun Park[3], Daehyun Baek[1], and Young-Yun Kong[1*].

[1]School of Biological Sciences, Seoul National University, 08826, Seoul, Korea.

[2]Molecular Recognition Research Center, Korea Institute of Science and Technology, Seoul, Republic of Korea.

[3]Graduate School of Medical Science and Engineering, KAIST, Daejeon, Republic of Korea.

[†] These authors contributed equally to this work.

[*] Corresponding author. Email: ykong@snu.ac.kr, Telephone: +82) 02-880-2638, FAX: +82) 02-872-1993

Author contributions:

Conceptualization, Y.L.K., Y.-W.J. and Y.-Y.K.; Data acquisition: Y.-W.J., Y.L.K., T.Y., J.-H.K. Y.-E.K., and S.-H.H.; Data analysis: Y.-W.J., Y.L.K., T.Y., and K.Y.; Technical support: T.Y., M.P., I.-W.S. J.-E.P., and D.B.; Writing: Y.L.K., Y.-W.J., T.Y., and Y.-Y.K.; Supervision: J.-E.P., D.B., Y.-Y.K.

Competing interests: Authors declare that they have no competing interests.

Abstract

Muscle stem cells (MuSCs) are parenchymal cells in skeletal muscle regeneration and maintenance. With aging, MuSCs experience a decline in their regenerative function and reduction in their number. However, recent evidence points to substantial heterogeneity within the aged MuSC population, raising questions about the underlying mechanisms of age-associated dysfunction. Here, we used Pax7^{CreERT2};Rosa^{YFP} mice (MuSC^{YFP}) to label Pax7-expressing MuSCs and chronologically traced MusCs until geriatric age. Genetic labeling and chronological tracing revealed that the number of YFP^{+} MuSC remained comparable between young, middle and geriatric ages. At geriatric age, YFP^{+} MuSCs exhibited reduced expression of traditional MuSC markers such as VCAM1 and PAX7. A previously unrecognized subpopulation emerged, characterized by loss of VCAM1 and low or absent PAX7. Despite their altered marker profile, these cells retained transcriptional signatures of quiescence and myogenic potential, but displayed significantly reduced proliferative and regenerative capacities. They displayed gene expression patterns indicative of senescence-like state and were selectively ablated by senolytic treatment. DHT restored regenerative function in aged mice and re-induced VCAM1 expression in YFP^{+}/Pax7$^{-/low}$/VCAM1^{-} cells, indicating responsiveness to rejuvenation. Based on their emergence with aging, functional impairment and responsiveness to rejuvenation, we termed this population GERI-MuSCs (Geriatric Emerging Rejuvenation-responsive and Impaired MuSCs). CD63 and CD200 were identified as novel surface markers that together with VCAM1, reliably detect GERI-MuSCs as well as classical Pax7^{+}/VCAM1^{High} MuSCs, providing a tool for comprehensive isolation of MuSCs from aged wild-type mice. Together, our findings provide a refined framework for studying MuSC aging and offer new tools for isolating functionally distinct MuSC subsets from aged skeletal muscle.

Introduction

Skeletal muscle regeneration is orchestrated primarily by tissue resident stem cells, known as muscle stem cells (MuSCs) or satellite cells(Relaix et al., 2021). MuSCs reside beneath the basal lamina of myofibers in a quiescent state under homeostatic condition but become rapidly activated upon injury to proliferate, differentiate, and fuse into regenerating myofibers(Evano and Tajbakhsh, 2018). While the regenerative function of MuSCs is well maintained in youth, a decline in their number and regenerative competence is observed in aging, leading to impaired muscle repair and tissue maintenance(Blau et al., 2015).

The age-related decline in MuSC function arises from a combination of extrinsic and intrinsic factors. Extrinsic factors include the increased pro-inflammatory cytokines(Degens, 2007), extracellular matrix remodeling(Schuler et al., 2021) and altered mechanical properties of the niche microenvironment(Chakkalakal et al., 2012). MuSC intrinsic factors include disrupted metabolic homeostasis(Pala et al., 2018), loss of proteostasis(Kim et al., 2021b), altered epigenetic regulation(Hernando-Herraez et al., 2019), mitochondrial dysfunction(Rygiel et al., 2016) and aberrant activation of signaling pathways, including p38 MAPK(Bernet et al., 2014), JAK/STAT(Price et al., 2014) and mTORC1(Tang et al., 2019). As a result, aged MuSCs show reduced colony-forming capacity, failure to maintain quiescence and loss of self-renewal potential causing a significant decline in the MuSC pool. This reduction in the resident stem cell population directly undermines the muscle's capacity for effective repair(Blau et al., 2015, Day et al., 2010).

Efforts to reverse MuSC dysfunction have explored both systemic and cell-intrinsic interventions. Circulating factors identified in parabiosis experiments(Conboy et al., 2005), as well as

68 supplementation with molecules such as NAD^+(Zhang et al., 2016) and oxytocin(Elabd et al.,
69 2014), have shown potential in restoring regenerative capacity. Pharmacological modulation of
70 signaling pathways, such as inhibition of JAK/STAT(Price et al., 2014), p38 MAPK(Bernet et al.,
71 2014), mTORC1, TGF-β(F and al., 2021), or Wnt signaling(AS and al., 2007), has led to improved
72 regeneration in aged muscle. However, variation in the age of experimental animals complicates
73 the interpretation of these findings. Many rejuvenation studies define 'aged' mice as 12 to 24
74 months old. This range encompasses a period of heterogeneous functional decline, during which a
75 substantial fraction of MuSCs may still retain regenerative capacity. Therefore, since it is unclear
76 whether these models fully represent a truly geriatric state, questions remain as to whether these
77 interventions directly restore dysfunctional MuSCs, selectively expand a subset of aged MuSCs
78 that retain partial functionality, or delay or prevent the aging of MuSCs that have not yet undergone
79 substantial aging. To address this uncertainty, we chronologically traced the fate of Pax7-
80 expressing MuSCs in geriatric mice using a genetic labeling system. This allowed us to evaluate
81 the composition, functionality, and responsiveness of aged MuSC subsets.

82 In addition to interventions aimed at reversing MuSC dysfunction, an alternative strategy to restore
83 regenerative competence involves targeting senescent cells. Senescent cells accumulate in aged
84 muscle and are thought to impair regeneration through secretion of pro-inflammatory and matrix-
85 remodeling factors, collectively known as the senescence-associated secretory phenotype (SASP)
86 (MJ and al., 2023, Saito and Chikenji, 2021). Senolytic agents, such as dasatinib and quercetin,
87 which selectively eliminate senescent cells have been shown to improve tissue homeostasis and
88 extend muscle healthspan in preclinical models(Xu et al., 2018). However, although senescence is
89 broadly defined as a state of irreversible cell cycle arrest accompanied by transcriptional
90 reprogramming, how this process manifests in quiescent adult stem cells *in vivo* remains

91 incompletely understood. This uncertainty raises concerns regarding the use of senolytics, as such
92 treatment may inadvertently eliminate MuSC subsets that retain latent regenerative potential. A
93 better understanding of how senescence-like features emerge within the aged MuSC pool is
94 therefore critical for evaluating the risks and benefits of senolytic treatment in aging muscle.

95 In this study, our findings reveal an age-dependent accumulation of a previously unrecognized
96 population of MuSCs, which we termed GERI-MuSCs (Geriatric Emerging Regeneration-
97 capable and Impaired MuSCs). GERI-MuSCs are characterized by low expression of traditional
98 marker genes, impaired yet retained functionality, susceptibility to senolytic deletion, and
99 responsiveness to DHT rejuvenation. Moreover, CD63 and CD200 can be reliable markers that
100 can be used with VCAM1 to detect previously hard-to-detect MuSCs. This combinatorial
101 strategy provides a framework for future isolation and therapeutic targeting of GERI-MuSCs.
102 Together, our results refine the understanding of in vivo MuSC aging and highlight the
103 importance of studying stem cell subsets that are functionally impaired yet not irreversibly
104 senescent.
105

106 **Results**

107 *Genetic labeling of Pax7^{+} cells reveal marker-deficient MuSCs in aged muscle*

108 *Paired box protein 7* (*Pax7*) is a transcription factor widely recognized as a defining marker of
109 MuSCs (Sambasivan et al., 2011). To investigate how aging alters the identity of MuSCs, we used
110 *Pax7^{CreERT2};Rosa^{YFP}* mice (MuSC^{YFP}). In this model, tamoxifen administration at 3-5 months of
111 age irreversibly labels Pax7-expressing MuSCs. YFP^{+} cells were isolated at young (3-5 months),
112 middle (10-14 months) and geriatric (>28 months) ages, using a conventional surface markers and

113 gating strategy: stem cell antigen-1 negative (SCA-1^{-}) and vascular cell adhesion protein 1 positive
114 (VCAM1^{+}) cells among lineage negative (CD31^{-}/CD45^{-}) and live cells (Liu et al., 2015) (Fig. 1A).
115 As previously reported, the number of VCAM1^{+}/SCA-1^{-} MuSCs declined significantly with age,
116 from an average of 12.22% at young and 13.62% at middle age to 8.31% at geriatric age (Fig. 1B).
117 Interestingly, however, when MuSCs were defined by YFP expression alone, their number
118 remained comparable across ages (Fig. 1C).
119
120 To investigate the disparity in the numbers of surface marker labelled MuSCs and genetically
121 labelled MuSCs at geriatric age, we examined the expression of traditional MuSC surface markers,
122 VCAM1 and integrin alpha 7 (ITGA7) in YFP^{+} population (Blanco-Bose et al., 2001, Sacco et al.,
123 2008). We observed a significant decline in VCAM1 expression, while ITGA7 expression
124 remained comparable (Fig. 1D). Notably, both VCAM1 and ITGA7 expression showed
125 significantly greater variation at geriatric age, in YFP^{+} cells, likely due to inter-individual
126 variability during aging.
127
128 Since YFP^{+} cells at geriatric age have varying marker gene expression, we investigated their
129 localization *in vivo* by conducting immunohistochemistry of *tibialis anterior* (TA) muscle sections
130 for PAX7. YFP^{+} cells showed sublaminar localization and co-expressed PAX7 in middle aged
131 mice (Fig. 1E). In geriatric aged mice, however, the number of PAX7^{+}/YFP^{+} cells decreased, while
132 YFP^{+}/PAX7$^{low/-}$ cells concomitantly increased (Fig. 1E).
133
134 To examine the relationship between PAX7 and varying MuSC marker expression, YFP^{+} cells
135 were grouped by VCAM1 expression levels: VCAM1^{High}, VCAM1^{Low}, and VCAM1^{-}, and

136 immunostained for PAX7. The PAX7 fluorescence intensity was comparable between VCAM1^{High}
137 cells from middle-aged and geriatric mice, but was markedly reduced in VCAM1^{Low} and VCAM1^{-}
138 cells of geriatric mice (Fig. 1F). Together, these findings show an emerging population of YFP^{+}
139 cells that lose traditional markers like Pax7 and VCAM1 at geriatric age.
140

141 *YFP^{+}/VCAM1^{-} cells are quiescent MuSCs*

142 To further explore the characteristics of YFP^{+}/VCAM1^{-} cells in geriatric mice, we examined their
143 potential myogenic status. Given that loss of canonical markers might reflect lineage progression,
144 we assessed the expression of myogenin (MYOG), a marker of late-stage myogenic differentiation,
145 in YFP^{+} cells from uninjured middle, geriatric ages and 5-days post injury. We found that MYOG
146 expression was largely absent in YFP^{+} cells from uninjured aged muscle, even in geriatric
147 YFP^{+}/VCAM1^{Low} and YFP^{+}/VCAM1^{-} cells (Fig. 2A-C). This contrasts with robust MYOG signal
148 detected at 5 days post injury, suggesting that YFP^{+} cells are not myoblasts.

149 To further investigate cell identity, we performed single-cell transcriptome analysis of YFP^{+} cells
150 from middle-aged and geriatric mice and integrated these data into public single-cell sequencing
151 data of uninjured and injured muscles.(De Micheli et al., 2020, Oprescu et al., 2020) (Fig. S1A-E).
152 Integration of public single-cell sequencing data yielded 5 clusters: quiescent MuSC, activated
153 MuSC, myoblast/myocyte, fast fiber myonuclei and slow fiber myonuclei (Fig. 2D). The
154 transcriptional signatures characterizing each cluster were consistent with known lineage identities,
155 supporting the validity of the clustering (Fig. 2E). Surprisingly, all YFP^{+} cells from both middle
156 and geriatric age mapped to transcriptional clusters associated with quiescent MuSCs (Fig. 2F).
157 This suggests that even VCAM1^{Low} and VCAM1^{-} cells from geriatric age did not cluster with

158 activated MuSCs or differentiating myoblasts or myocytes, but rather remained within the
159 quiescent MuSC compartment. These findings support the possibility that these cells may retain
160 core stem-like features, despite altered surface marker profiles.

161 Since quiescent MuSCs are generally smaller than activated progenitors due to reduced
162 cytoplasmic volume, low metabolic activity, and compact chromatin organization(Liu et al., 2013),
163 we also compared the cell size of VCAM1^{-} cells with activated MuSCs from injured mice. Indeed,
164 both VCAM1^{Low} and VCAM1^{-} cells from geriatric mice were similar in diameter to YFP^{+} cells
165 from uninjured middle aged mice, but were significantly smaller than activated MuSCs from
166 injured mice (Fig. S2A-B). These results are consistent with our interpretation that VCAM1^{Low}
167 and VCAM1^{-} cells from geriatric mice may remain in a quiescent state.

168 Given reports of smooth muscle mesenchymal cells (SMMCs) expressing overlapping surface
169 markers with MuSCs, we considered whether the VCAM1^{-} cells might reflect SMMC
170 contamination(Giordani et al., 2019). mRNA sequence analysis revealed that this population
171 exhibited low expression of SMMC markers, including Myl9, Acta2, and Pdgfrb (Fig S2C),
172 suggesting they are transcriptionally distinct from SMMCs. Together, these results suggest that
173 YFP^{+}/VCAM1^{-} cells from geriatric age may retain quiescent features and myogenic identity,
174 despite lacking typical MuSC markers.

175

176 *Impaired functionality of YFP^{+}/VCAM1^{-} MuSCs*

177 Since YFP^{+}/VCAM1^{-} cells retained molecular and morphological features consistent with
178 quiescent MuSCs, we next investigated their functional potential. Colony-forming assays revealed
179 that YFP^{+}/VCAM1^{High} cells from geriatric mice expanded at comparable rates to those from

180 middle-aged mice. In contrast, colony formation by $YFP^{+}/VCAM1^{Low}$ and $YFP^{+}/VCAM1^{-}$ subsets
181 were progressively reduced, with the $VCAM1^{-}$ subsets forming smaller colonies (Fig. 3A-B).
182 These findings suggest that these cells retain proliferative ability, although their expansion
183 capacity was compromised.

184 To examine their regenerative potential *in vivo*, we transplanted equal numbers of YFP^{+} cells from
185 each group into pre-injured TA of MuSC-deficient *Pax7*^{CreERT2};*Rosa*^{DTA} recipient mice (Fig. 3C).
186 In the absence of donor cells, regeneration was severely impaired, consistent with a lack of
187 endogenous MuSCs (Fig 3D). Transplantation of $YFP^{+}/VCAM1^{High}$ cells from both middle-aged
188 and geriatric donors supported robust regeneration, resulting in centrally nucleated myofibers with
189 comparable morphology between age groups, consistent with heterotypic transplantation studies
190 (Fig. 3D-E) (Ikemoto-Uezumi et al., 2015).

191 Interestingly, both $YFP^{+}/VCAM1^{Low}$ or $YFP^{+}/VCAM1^{-}$ cells were also capable of contributing to
192 myofiber regeneration, despite lacking traditional MuSC markers (Fig. 3E). However, regenerated
193 myofibers in these groups were significantly smaller than those derived from $VCAM1^{High}$ cells
194 (Fig. 3F), suggesting that loss of VCAM1 expression may be associated with diminished
195 regenerative capacity.

196 Together, these results indicate that even the most marker-deficient MuSCs in geriatric muscle,
197 $YFP^{+}/VCAM1^{-}$ cells, retain a degree of regenerative competence. However, their reduced
198 proliferative output and attenuated *in vivo* contribution suggests functional heterogeneity within
199 the aged MuSC pool, wherein diminished marker expression may correlate with impaired
200 regenerative performance.

201

202 *VCAM1⁻ MuSCs exhibit senescence-like features and sensitivity to senolytics*

203 To investigate the molecular basis of impaired function in VCAM1^{-} MuSCs, we performed mRNA
204 sequence analysis on YFP^{+} MuSCs. Samples showed high quality and a strong correlation was
205 observed among biological replicates (Fig. S3A-C). Each group consistently reproduced similar
206 gene expression patterns in biological replicates in hierarchical clustering (Fig. S3D). In particular,
207 hierarchical clustering showed similar gene expression pattern between VCAM1^{High} MuSCs of
208 middle-aged and geriatric mice and between VCAM1^{Low} and VCAM1^{-} MuSCs (Fig. S3E),
209 consistent with our results of *in vivo* and *in vitro* functionality experiments (Fig. 3A-F).

210 Kyoto-encyclopedia of genes and genomes (KEGG) pathway enrichment analysis based on the
211 DEGs (Fig. S4E) (Kolberg et al., 2023) showed alterations in pathways related to cellular
212 senescence and PI3K-AKT pathway in VCAM1^{-} MuSCs of geriatric age as compared to
213 VCAM1^{High} MuSCs of middle-age (Fig. 4A). We further investigated the expression levels of
214 individual genes known to be altered in MuSCs of aged mice, such as genes related to extracellular
215 matrix (Schuler et al., 2021), Notch signaling (Liu et al., 2018, Conboy et al., 2003, Conboy et al.,
216 2005), and autophagy-lysosomal pathway (Garcia-Prat et al., 2016, Kim et al., 2021b), all of which
217 were more altered in VCAM1^{Low} and VCAM1^{-} MuSCs compared to VCAM1^{High} MuSCs of
218 geriatric mice (Fig. 4B). *Cdkn2a* (*p16^{INK4a}*) and *Cdkn2b* (*p15^{INK4b}*), which are cell cycle regulators
219 widely used as markers for senescent cells, showed highly altered expression patterns in VCAM1^{-}
220 MuSCs compared to VCAM1^{Low} MuSCs (Fig. 4B) (Saito and Chikenji, 2021). However, the
221 expression levels of other well-known cellular senescence marker genes, such as *Rb1*, *Il6*, and
222 *Trp53*, were not altered much. *Pik3cb* and *Tsc1,* which are involved in the PI3K-Akt-mTOR
223 pathway, showed overall increased expression, while other genes in the PI3K-Akt pathway

224 remained relatively unchanged. Together, these results suggest a unique combination of *in vivo*
225 senescence-like molecular characteristics of VCAM1^{-} MuSCs, distinct from molecular
226 characteristics of replicative cellular senescence.

227 Given their unique senescence associated transcriptome and partially elevated PI3K-Akt pathway,
228 we tested whether VCAM1^{-} MuSCs were susceptible to senolytic elimination. Geriatric mice were
229 treated with senolytic agents dasatinib and quercetin (DQ) (Xu et al., 2018), and analyzed 2 weeks
230 later (Fig. 4C). Despite variation in baseline VCAM1^{High} and VCAM1$^{Low/-}$ population across aged
231 animals, a consistent inverse correlation was observed between VCAM1^{High} and VCAM1$^{Low/-}$
232 fractions (Fig. S3F). Following DQ treatment, VCAM1^{High} MuSCs remained comparable while
233 VCAM1$^{Low/-}$ MuSCs showed reduced abundance and lower variability (Fig. 4D). These results
234 indicate selective sensitivity of VCAM1$^{Low/-}$ MuSCs to senolytic agents.

235 Together, our findings reveal a distinct subset of quiescent MuSCs in geriatric muscle that exhibit
236 unique senescence-like molecular features and are amenable to senolytic clearance. We term these
237 cells GERI-MuSCs (Geriatric Emerging Regeneration-capable and Impaired-MuSCs).

238

239 *Rejuvenation of GERI-MuSCs by DHT treatment*

240 Studies have demonstrated that treatment with rejuvenating agents can restores myofiber
241 regeneration capacity in aged mice (Bernet et al., 2014, Cosgrove et al., 2014, Zhang et al., 2016,
242 Elabd et al., 2014, Price et al., 2014, Garcia-Prat et al., 2016). Previously, dihydrotestosterone
243 (DHT) supplementation has been shown to preserve MuSCs function and enhance regeneration in
244 antide treated mice by restoring autophagy activation (Kim et al., 2021b). Consistent with these

245 findings, implantation of DHT-filled silastic tube in 28-month-old geriatric mice improved muscle
246 regeneration, as evidenced by increased fiber cross sectional area (Fig. S4A-C).

247 To investigate whether DHT could affect GERI-MuSCs, we treated 28-month-old MuSC^{YFP} mice
248 with DHT and analyzed MuSC populations one month later (Fig. 4E). Remarkably, DHT treatment
249 resulted in a decrease in GERI-MuSCs with a corresponding expansion of VCAM1^{High} MuSCs
250 population. This phenotypic reversion suggests that DHT promotes restoration of canonical marker
251 expression in GERI-MuSCs.

252 To determine whether DHT acts through rejuvenation of GERI-MuSCs, we first depleted these
253 cells using DQ, then administered DHT. In mice pre-treated with DQ, DHT supplementation failed
254 to reconstitute the VCAM1^{High} MuSC pool (Fig. 4F). This finding suggests a model in which
255 GERI-MuSCs are not terminally senescent, but rather exist in a latent, hormone-responsive state.
256 Upon DHT exposure, these cells likely reacquire a Vcam1^{High} phenotype, underscoring their
257 potential as a therapeutic target in muscle aging.

258

259 *Identification of GERI-MuSCs using CD63 and CD200*

260 In non-reporter models, the detection and isolation of GERI-MuSCs pose a significant challenge,
261 as these cells lack expression of conventional MuSC markers such as VCAM1 and PAX7 at
262 geriatric age. To overcome this limitation, we conducted a transcriptomic screen to identify
263 alternative surface markers that remain stably expressed across the full spectrum of MuSC aging
264 states. Candidate genes were selected based on three criteria; high transcript abundance (RPKM),
265 consistent expression from VCAM1^{High} to VCAM1^{-} MuSCs, and predicted surface localization.

266 CD63 and CD200 sufficed all three criteria and were therefore chosen as candidate markers for
267 further validation (Fig. 5B).

268 We confirmed protein level expression of CD63 and CD200 expression in MuSCs by we co-
269 immunostaining TA cross-sections for CD63, CD200, YFP and PAX7. Both markers co-localized
270 with YFP and PAX7 beneath the basal lamina (Fig. 5C, D). Flow cytometry analysis further
271 demonstrated that 96.3% of $YFP^{+}/VCAM1^{+}$ cells from young $MuSC^{YFP}$ mice were
272 $CD63^{high}/CD200^{high}$ (Fig. 5E). Notably, among lineage-negative ($CD31^{-}/CD45^{-}$), SCA-1^{-}, and live
273 cells, 93.2% of $CD63^{high}/CD200^{high}$ cells were $YFP^{+}/VCAM1^{+}$ cells (Fig. 5F). Importantly,
274 96.5±2.8% of sorted $CD63^{high}/CD200^{high}$ cells were $PAX7^{+}$, validating these markers as a robust
275 strategy for MuSC enrichment.

276 To assess whether the CD63/CD200-based strategy could detect and isolate GERI-MuSCs in wild-
277 type mice, we applied the strategy to middle and geriatric aged mice. In middle aged mice, all
278 $CD63^{high}/CD200^{high}$ cells corresponded exclusively to $VCAM1^{High}$ MuSCs (Fig. 5H). In contrast,
279 geriatric mice exhibited a marked shift, with the majority of $CD63^{high}/CD200^{high}$ cells falling
280 within the $VCAM1^{Low/-}$ gate (Fig. 5H). These results indicate that CD63 and CD200 expression is
281 preserved in GERI-MuSCs, enabling their prospective identification and isolation in the absence
282 of genetic labeling. Therefore, these findings establish CD63 and CD200 as reliable surface
283 markers that can be used with VCAM1. Together, they can to detect the full spectrum of MuSCs,
284 including functionally latent populations that evade detection by conventional means. This strategy
285 offers a critical tool for future studies aiming to comprehensively characterize MuSC heterogeneity
286 and therapeutic responsiveness in the context of aging.

287

288 **Discussion**

289 Our study challenges the longstanding paradigm that muscle stem cell (MuSC) number declines
290 irreversibly with age. While previous reports have described significant depletion of Pax7^{+} MuSCs
291 in aged muscle, these findings were largely based on immunohistochemical detection or flow
292 cytometric profiling using conventional surface markers. Here, we demonstrate that genetically
293 labeled MuSCs, tracked longitudinally *in vivo* using a Pax7-CreERT2;Rosa-YFP model, do not
294 decrease in number even in geriatric mice. Instead, a substantial subset of aged MuSCs loses
295 expression of canonical markers such as Pax7 and VCAM1, rendering them undetectable by
296 traditional approaches.

297 We identify this overlooked population as GERI-MuSCs (Geriatric Emerging Regeneration-
298 capable and Impaired MuSCs). Despite their diminished expression of hallmark MuSC markers,
299 GERI-MuSCs exhibit features consistent with quiescence, rather than terminal differentiation or
300 apoptosis. Transcriptomic profiling and functional assays reveal that these cells retain a partial
301 capacity for proliferation and regeneration, albeit at reduced efficiency. These findings suggest
302 that previous conclusions about MuSC depletion may have reflected loss of marker expression
303 rather than true cellular loss.

304 GERI-MuSCs display a unique gene expression profile that includes upregulation of senescence-
305 associated transcripts such as Cdkn2a but unaltered expression of other typical senescence-
306 associated genes, such as Il6 and Mmp3, while showing preservation of certain stemness-related
307 pathways. These cells do not fulfill the classical definition of cellular senescence, such as
308 irreversible cell cycle arrest. Rather, GERI-MuSCs exhibit a hybrid state—retaining regenerative
309 potential while expressing select markers traditionally associated with senescence. This finding

310 suggests that the criteria used to define senescence in proliferative cell types may not fully apply
311 to quiescent stem cells like MuSCs, which spend most of their life in a non-proliferative state.
312 Further studies are warranted to delineate *in vivo* senescence features specific to long-lived, tissue-
313 resident stem cells.

314 Our results suggest that GERI-MuSCs could be functionally reactivated. Treatment with
315 dihydrotestosterone (DHT) restored VCAM1 expression in GERI MuSCs and regenerative
316 performance in aged mice, suggesting that their phenotype is reversible and hormonally responsive.
317 This provides a compelling explanation for the efficacy of hormone-based interventions in aging
318 muscle and highlights the potential for targeting latent regenerative capacity in aged stem cells.
319 Notch signaling appears to be a key regulator of this reversible phenotype. We found diminished
320 expression of Notch pathway components—including Notch1, Notch3, Hey1, and HeyL—in
321 VCAM1Low and VCAM1– subsets, along with reduced transcription of Pax7 and VCAM1. Given
322 that both Pax7 and VCAM1 are downstream targets of Notch signaling and that Notch activity can
323 be modulated by androgen signaling, the restoration of MuSC function by DHT may act through
324 this axis. Testing such mechanisms in future studies will be important for establishing therapeutic
325 strategies.

326 The presence of GERI-MuSCs also raises caution about the use of senolytic agents. Although
327 dasatinib and quercetin are used to clear senescent cells and have shown benefits in aged tissue,
328 our data show that these agents also deplete GERI-MuSCs. Since GERI-MuSCs retain
329 functionality and regenerative potential, their removal could compromise muscle maintenance and
330 repair in elderly individuals. Given the critical role of MuSCs in preserving muscle mass,

331 supporting myonuclei turnover, and maintaining neuromuscular junctions, the long-term
332 application of senolytics in skeletal muscle warrants careful scrutiny.

333 Finally, we propose CD63 and CD200 as reliable surface markers that can be used with VCAM1
334 for identifying MuSCs across age groups. These markers remain expressed in both young and aged
335 MuSCs, including those with diminished canonical marker expression. Their use enables
336 comprehensive isolation of the full MuSC population and will be instrumental in improving the
337 resolution of future studies on stem cell heterogeneity and aging.

338 In conclusion, we identify a previously unrecognized population of MuSCs—GERI-MuSCs—that
339 persists with age despite loss of conventional markers. These cells remain quiescent, partially
340 functional, and responsive to rejuvenation cues. Their discovery challenges existing models of
341 MuSC depletion and senescence, and underscores the importance of revisiting stem cell aging with
342 improved detection strategies and nuanced interpretations of cellular function.

343 **Materials and Methods**

344 ***List of Antibodies for Flow Cytometry and FACS (Fluorescence-activated cell sorting***

Marker	Fluorophore	Catalog No.	Company
CD31	APC	102510	BioLegend
CD31	Pacific Blue™	108120	BioLegend
CD45	APC	103112	BioLegend
CD45	Pacific Blue™	405206	BioLegend
VCAM1	Biotin	553331	BD Biosciences
Streptavidin	PE/Cy7	405206	BioLegend
Ly-6A/E (Sca-1)	Pacific Blue™	108120	BioLegend
Ly-6A/E (Sca-1)	FITC	553335	BD Biosciences
CD200	BV711	745548	BD Biosciences
CD63	APC	170631-82	eBioscience

345

346 ***Animals***

347 All animal procedures conformed to the guidelines of Institutional Animal Care and Use
348 Committee (IACUC) of Seoul National University, Korea. Male C57BL/6J mice were housed
349 under a 12-h light/12-h dark cycle at 22°C with 40-60% humidity, and fed ad libitum. Pax7^{CreER}
350 (017763), Rosa^{YFP} (006148), Rosa^{DTA} (009669) mice were obtained from the Jackson Laboratory
351 (Bar, Harbor, ME, USA). Tamoxifen (25mg/mL in corn oil; Sigma-Aldrich, St. Louis, MO, USA)
352 was administered orally for 5 consecutive days (240 mg/kg). For muscle injury, mice were
353 anesthetized with avertin (250 μg/g, i.p.) and injected with 60 μL of 1.2% BaCl2 (Sigma-Aldrich)

354 into the Tibialis Anterior (TA) muscles. One-day post-injury, mice were anesthetized with avertin
355 and MuSCs were transplanted at indicated numbers.
356
357 ***Flow Cytometry and FACS (Fluorescence-activated cell sorting)***
358 Limb muscles were mechanically dissected and enzymatically dissociated in Dulbecco's modified
359 Eagle's medium (DMEM) containing 10% horse serum (Hyclone, Logan, UT, USA), collagenase
360 type II (800U/mL; Worthington, Lakewood, NJ, USA), and dispase (1.1 U/mL; StemCell
361 Technologies, Vancouver, BC, Canada) at 37°C for 50 minutes. Digested suspensions were
362 triturated, washed with DMEM and filtered to obtain mononuclear cells. Cells were stained with
363 antibodies, analyzed and sorted using a FACS Aria III or FACS Aria Fusion (BD Bioscience). List
364 of antibodies used are provided as supplementary materials. Representative plots were processed
365 with FlowJo v10.9.
366
367 ***MuSC Culture***
368 FACS-isolated MuSCs were cultured in DMEM/F12 + 20% FBS + 1% ZellShield (Minerva
369 Biolabs, Germany) + 2.5 ng/mL bFGF (F0291, Sigma Aldrich) on Matrigel (256231, BD
370 Bioscience)-coated plates at 37°C and 5% CO_2. Medium was refreshed every 3 days. MuSCs were
371 imaged daily using EVOS FL Auto 2 (Thermo Fisher, USA) and the number of cells in the same
372 region was counted.
373
374 ***Histochemistry and Immunohistochemistry***
375 TA muscles were fixed overnight in 4% paraformaldehyde, embedded in the Tissue Tek OCT
376 compound (Sakura Fineteck, USA), and snap-frozen in liquid nitrogen. The muscles were

377 sectioned at 7μm and stained on the slides. H&E staining was performed according to basic
378 protocols. For immunostaining, sections were subjected to epitope retrieval in 50mM Tris-EDTA
379 (pH 9.0) at 105°C for 10 minutes, then blocked with 3% BSA + 0.1% Triton X-100. Sections were
380 incubated overnight with primary antibodies, mouse anti-PAX7 (DSHB, Pax7, 1:100 dilution),
381 chicken anti-GFP (abcam, ab13970, 1:300), rabbit anti-laminin (Sigma, L9393-2ML, 1:500), rat
382 anti-CD200 (BD Biosciences, 1:50), and rat anti-CD63 (eBioscience, 1:50). After washing,
383 sections were incubated with secondary antibodies, Alexa Fluor 647-conjugated anti-rat or anti
384 rabbit IgG, Alexa Fluor 594-conjugated anti mouse IgG, and Alexa Fluor 488-conjugated anti
385 chicken IgG. Nuclei were counterstained with Hoechst 33342 (Invitrogen, H3570). Slides were
386 mounted with VECTASHIELD (Vector Laboratories) and images were acquired using EVOS FL
387 Auto 2 (Thermo Fisher) and Leica TCS SP8 confocal microscope. Cross-sectional area (CSA) was
388 calculated by SMASH[23] and ImageJ programs, respectively.
389
390 ***Immunocytochemistry***
391 Isolated MuSCs were cytospun onto slides (Cytospin 4, Thermo Scientific), fixed with 4%
392 paraformaldehyde for 10 minutes, washed with PBS and permeabilized with PBS containing 0.4%
393 Triton X-100 for 30 minutes. Slides were then incubated with primary antibodies, mouse anti-
394 PAX7 (DSHB) and mouse anti-MYOG (DSHB, F5D, 1:100 dilution) in blocking buffer.
395 Subsequent steps followed the immunohistochemistry protocol. Relative fluorescent intensity was
396 quantified using ImageJ.
397
398 ***Senolytics and DHT treatment***

399 Dihydrotestosterone (DHT) implantation was performed as previously described[8]. Senolytic
400 agents Dasatinib (D-3307, LC laboratories, 5mg/kg) and Quercetin (Q4951, Sigma, 50 mg/kg) was
401 administered orally for 5 consecutive days. Experimental schemes of combined treatment are as
402 mentioned in the results section of this article.
403
404 ***Single-cell RNA sequence analysis***
405 To obtain gene-specific UMI (Unique Molecular Identifier) counts in each cell, we processed raw
406 scRNA-seq data using the BD Rhapsody WTA analysis pipeline (v1.11.1)[24]. Scanpy (v1.9.3)[25]
407 was utilized for single-cell RNA sequence analysis. Cells with a gene count below 200 or a
408 mitochondrial gene percentage above 20% were considered low-quality cells and were excluded
409 from downstream analyses. We set the upper limit of each UMI count as (mean(total counts) + 2
410 standard deviation(total counts) value) to remove doublets. Normalization was applied to the count
411 matrix (scanpy.pp.normalize_total with target_sum=10^4 and scanpy.pp.log1p).
412 We characterized the enriched cells by merging our scRNA-seq data with public datasets
413 (GSE162172, GSE138826)[26,27]. From the public dataset, only the cells belonging to the
414 myogenic lineage (from quiescent MuSCs to Myonuclei (Type IIb or IIx)) were selected for
415 comparison. After merging the public dataset with our dataset
416 (scanpy.external.pp.harmony_integrate with max_iter_harmony=50), 2000 highly variable genes
417 were identified and scaled (scanpy.pp.highly_variable_genes with n_top_genes=2000,
418 scanpy.pp.scale with max_value=10).
419 We visualized the scRNA-seq data using uniform manifold approximation and projection (UMAP)
420 (scanpy.tl.umap) with a precomputed neighborhood graph (scanpy.pp.neighbors with n_pcs=50).
421 We clustered the UMAP-transformed data using the Louvain algorithm (scanpy.tl.louvain,

422 resolution=0.5). Each cluster was annotated using cell-specific markers (Fig. 1D, E). The
423 proportions of quiescent MuSCs, activated MuSCs, and Myoblasts/Progenitors were measured in
424 our samples (Mid and Geri) and the public dataset across various days-post-injury (DPI). Cases
425 with less than 50 cells per DPI were excluded during this analysis (Fig. S1A).
426 We utilized diffusion map, PAGA, and force-directed graph to analyze the trajectory of cells
427 belonging to the myogenic lineage. After dimension reduction using diffusion maps
428 (scanpy.tl.diffmap), we computed neighborhood graphs (scanpy.pp.neighbors) and abstracted the
429 graphs using PAGA (scanpy.tl.paga). We modeled the trajectory of the cells using the abstracted
430 graphs as initial positions by constructing a force-directed graph (Fig. S1B-E).
431
432 ***Representative Isoforms of Mouse mRNAs***
433 To acquire a sole representative isoform for each gene, we utilized the filtering pipeline described
434 in a previous study(Kim et al., 2016). The mouse reference annotation (GRCm39 refFlat) was
435 downloaded from the UCSC website(Pruitt et al., 2007). mRNA sequences with accession
436 category 'NM' located on the 21 chromosomes (1-19, X, and Y) were selected for downstream
437 analyses. Entries with incorrect start or stop codons, internal stop codons, and ORF lengths not
438 divisible by 3, were removed. Nonsense-mediated mRNA decay candidates, defined as the
439 mRNAs with stop codons positioned less than 50 nucleotides before the final exon-exon junction,
440 were excluded (Nagy and Maquat, 1998). A total of 20,582 non-redundant representative isoforms
441 were selected as mouse reference mRNAs for subsequent analyses.
442
443 ***mRNA sequence analysis***

444 We trimmed low-quality read ends using a custom algorithm. Each base position was assigned a
445 reward (+5) or a penalty (-1) based on its Phred score with a threshold of 30. To define high-quality
446 read ends, we calculated the cumulative sum from both ends, identified the positions with the
447 minimum value, and trimmed the reads at those positions. This process was repeated iteratively
448 until no further trimming was necessary. Reads shorter than 17 bases after trimming were excluded.
449 Subsequently, we removed adapter sequences using Cutadapt (v3.1) (Martin, 2011) with options
450 (-O 10 -m 18 --match-read-wildcards). We eliminated sequencing artifacts and PCR duplicates
451 using FASTX-Toolkit's fastx_artifact_filter with option (-Q 33) (hannonlab.cshl.edu/fastx_toolkit/,
452 v0.0.13). To eliminate reads derived from mouse non-coding RNA, we aligned the reads to non-
453 coding RNA sequences in RNAcentral(Consortium, 2021) using Bowtie2 (v2.1.0) (Langmead and
454 Salzberg, 2012) with options (-k 1 --norc --very-sensitive), and the reads aligned to non-coding
455 RNAs were excluded. Unpaired reads were also excluded.
456 Preprocessed reads were aligned to the mouse genome (GRCm39) utilizing the STAR alignment
457 software (v2.7.5b) (Dobin et al., 2013). The parameters used for the STAR alignment are described
458 in a previous study (Kim et al., 2021a). The reads were sorted and indexed using Samtools (v0.1.19)
459 (Danecek et al., 2021). The expression of each gene was quantified by calculating the fragment
460 per kilobase of transcript per million mapped reads (FPKM).
461 We applied the same analysis pipeline to both our experimental samples (Mid, Vh, Vl, V-) and
462 publicly available SMMC samples (GSE110878, SRR67542132-SRR67542134)(Giordani et al.,
463 2019) to calculate gene expression levels. Quantile-normalized expression levels were compared
464 between the two datasets (Fig. S2C).
465 The following analyses were performed exclusively on our experimental samples.

466 To assess the quality of our samples, the proportion of reads that were either removed, unmapped,
467 or successfully mapped was computed for each sample throughout the preprocessing and
468 alignment steps (Fig. S3B). The correlation between replicates was quantified using Spearman's
469 R (Fig. S3C).
470 We normalized all samples using the following procedure to ensure a fair inter-sample comparison.
471 We applied quantile normalization to equalize the FPKM distribution of all samples. To remove
472 individual mouse variations, we used the RUVs function (k=2) from the RUVSeq package (v1.34.0)
473 (Risso et al., 2014). Subsequently, genes with normalized expression higher than the 50th percentile
474 were selected, and the expression values were z-normalized. We clustered the samples using the
475 clustermap function of the Seaborn package (v0.11.1) (Waskom, 2021) with correlation metric
476 (Fig. S3D).
477 We identified differentially expressed genes (DEGs) by comparing the expression between the
478 Mid, V^H, V^L, and V^- samples. We used DESeq2 (v1.40.2) (Love et al., 2014) to compute $\log_2$ fold
479 changes and false discovery rate (FDR) corrected *Q* values for individual genes. DEGs were
480 defined as genes with $|\log_2$ fold change$| > 1.2$ and FDR-corrected *Q* value < 0.05 (Fig. S3E).
481 To annotate the pathways linked to DEGs, we performed enrichment analysis for Kyoto
482 Encyclopedia of Genes and Genomes (KEGG) pathways using the g:Profiler web server (Kolberg
483 et al., 2023, Kanehisa et al., 2016). Among the highly expressed 12,000 genes, DEGs were queried
484 using the g:GOst tool, and the g:SCS algorithm was employed for multiple testing correction.
485 Pathways with multiple testing corrected *Q* value < 0.05 were presented (Fig. 3A).
486
487 ***Statistical Analysis***

488 All statistical analyses were performed using R (R-4.3.1) and GraphPad Prism. All variables were
489 confirmed to have a normal distribution by using the Shapiro-Wilk test and Kolmogorov-Smirnov
490 test. For comparison of significant differences in 2 groups of normally distributed data, Levene's
491 test for homogeneity of variance using the car package followed by a 2-tailed Student's *t* test or
492 Welch's *t* test was used. For comparison of multiple groups, one-way analysis of variance
493 (ANOVA) or two-way ANOVA followed by Bonferroni's multiple comparison test was
494 performed. All data are presented as mean ± s.d. n.s., not significant; P > 0.05; *P <0.05; **P<0.01;
495 ***P<0.001, ****P<0.0001. *P value* of <.05 considered statistically significant at the 95%
496 confidence level. The number of biological replicates, *p* values, and detailed statistical method for
497 each data were indicated in the figure legends.
498

499 **Acknowledgments**

500 We thank C.Kang (Seoul National University) for providing senolytic agents, Dasatinib and
501 Quercetin.
502

503 **Funding**

504 This work was supported by the National Research Foundation of Korea (NRF) grant funded by
505 the Korea government (MIST) (RS-2020-NR049538)
506

507 **Data and materials availability:** The bulk RNA sequencing data and scRNA-seq data have been
508 deposited at Gene Expression Omnibus (GEO, GSE accession number: GSE254475 and
509 GSE254476, respectively) and are publicly available as of the date of publication. Source data

supporting the findings of this study are provided with this paper. Additional data that support the findings of this study are available from the corresponding author upon reasonable request.

512 **References**

513 AS, B. & AL., E. 2007. Increased Wnt signaling during aging alters muscle stem cell fate and
514 increases fibrosis. *Science,* 317**,** 807–810.

515 BERNET, J. D., DOLES, J. D., HALL, J. K., KELLY TANAKA, K., CARTER, T. A. & OLWIN,
516 B. B. 2014. p38 MAPK signaling underlies a cell-autonomous loss of stem cell self-renewal in
517 skeletal muscle of aged mice. *Nat Med,* 20**,** 265-71.

518 BLANCO-BOSE, W. E., YAO, C. C., KRAMER, R. H. & BLAU, H. M. 2001. Purification of
519 mouse primary myoblasts based on alpha 7 integrin expression. *Exp Cell Res,* 265**,** 212-20.

520 BLAU, H. M., COSGROVE, B. D. & HO, A. T. 2015. The central role of muscle stem cells in
521 regenerative failure with aging. *Nat Med,* 21**,** 854-62.

522 CHAKKALAKAL, J. V., JONES, K. M., BASSON, M. A. & BRACK, A. S. 2012. The aged niche
523 disrupts muscle stem cell quiescence. *Nature,* 490**,** 355-60.

524 CONBOY, I. M., CONBOY, M. J., SMYTHE, G. M. & RANDO, T. A. 2003. Notch-mediated
525 restoration of regenerative potential to aged muscle. *Science,* 302**,** 1575-7.

526 CONBOY, I. M., CONBOY, M. J., WAGERS, A. J., GIRMA, E. R., WEISSMAN, I. L. &
527 RANDO, T. A. 2005. Rejuvenation of aged progenitor cells by exposure to a young systemic
528 environment. *Nature,* 433**,** 760-4.

529 CONSORTIUM, T. R. 2021. RNAcentral 2019: a hub of information for non-coding RNA
530 sequences. *Nucleic Acids Res,* 49**,** D212-D220.

531 COSGROVE, B. D., GILBERT, P. M., PORPIGLIA, E., MOURKIOTI, F., LEE, S. P., CORBEL,
532 S. Y., LLEWELLYN, M. E., DELP, S. L. & BLAU, H. M. 2014. Rejuvenation of the muscle stem
533 cell population restores strength to injured aged muscles. *Nat Med,* 20**,** 255-64.

534 DANECEK, P., BONFIELD, J. K., LIDDLE, J., MARSHALL, J., OHAN, V., POLLARD, M. O.,
535 WHITWHAM, A., KEANE, T., MCCARTHY, S. A., DAVIES, R. M. & LI, H. 2021. Twelve
536 years of SAMtools and BCFtools. *Gigascience,* 10.

537 DAY, K., SHEFER, G., SHEARER, A. & YABLONKA-REUVENI, Z. 2010. The depletion of
538 skeletal muscle satellite cells with age is concomitant with reduced capacity of single progenitors
539 to produce reserve progeny. *Dev Biol,* 340**,** 330-43.

540 DE MICHELI, A. J., LAURILLIARD, E. J., HEINKE, C. L., RAVICHANDRAN, H., FRACZEK,
541 P., SOUEID-BAUMGARTEN, S., DE VLAMINCK, I., ELEMENTO, O. & COSGROVE, B. D.
542 2020. Single-Cell Analysis of the Muscle Stem Cell Hierarchy Identifies Heterotypic
543 Communication Signals Involved in Skeletal Muscle Regeneration. *Cell Rep,* 30**,** 3583-3595 e5.

544 DEGENS, H. 2007. The role of systemic inflammation in age-related muscle wasting and
545 reparation. *J Physiol,* 583**,** 343--344.

546 DOBIN, A., DAVIS, C. A., SCHLESINGER, F., DRENKOW, J., ZALESKI, C., JHA, S., BATUT,
547 P., CHAISSON, M. & GINGERAS, T. R. 2013. STAR: ultrafast universal RNA-seq aligner.
548 *Bioinformatics,* 29**,** 15-21.

549 ELABD, C., COUSIN, W., UPADHYAYULA, P., CHEN, R. Y., CHOOLJIAN, M. S., LI, J.,
550 KUNG, S., JIANG, K. P. & CONBOY, I. M. 2014. Oxytocin is an age-specific circulating
551 hormone that is necessary for muscle maintenance and regeneration. *Nat Commun,* 5**,** 4082.

552 EVANO, B. & TAJBAKHSH, S. 2018. Skeletal muscle stem cells in comfort and stress. *NPJ*
553 *Regen Med,* 3**,** 24.

554 F, G. & AL., E. 2021. TGFβ signaling curbs cell fusion and muscle regeneration. *Nature*
555 *Communications,* 12**,** 3131.

556 GARCIA-PRAT, L., MARTINEZ-VICENTE, M., PERDIGUERO, E., ORTET, L.,
557 RODRIGUEZ-UBREVA, J., REBOLLO, E., RUIZ-BONILLA, V., GUTARRA, S.,
558 BALLESTAR, E., SERRANO, A. L., SANDRI, M. & MUNOZ-CANOVES, P. 2016. Autophagy
559 maintains stemness by preventing senescence. *Nature,* 529**,** 37-42.

560 GIORDANI, L., HE, G. J., NEGRONI, E., SAKAI, H., LAW, J. Y. C., SIU, M. M., WAN, R.,
561 CORNEAU, A., TAJBAKHSH, S., CHEUNG, T. H. & LE GRAND, F. 2019. High-Dimensional
562 Single-Cell Cartography Reveals Novel Skeletal Muscle-Resident Cell Populations. *Mol Cell,* 74**,**
563 609-621 e6.

564 HERNANDO-HERRAEZ, I., EVANO, B., STUBBS, T., COMMERE, P. H., JAN BONDER, M.,
565 CLARK, S., ANDREWS, S., TAJBAKHSH, S. & REIK, W. 2019. Ageing affects DNA
566 methylation drift and transcriptional cell-to-cell variability in mouse muscle stem cells. *Nat*
567 *Commun,* 10**,** 4361.

568 IKEMOTO-UEZUMI, M., UEZUMI, A., TSUCHIDA, K., FUKADA, S., YAMAMOTO, H.,
569 YAMAMOTO, N., SHIOMI, K. & HASHIMOTO, N. 2015. Pro-Insulin-Like Growth Factor-II
570 Ameliorates Age-Related Inefficient Regenerative Response by Orchestrating Self-Reinforcement
571 Mechanism of Muscle Regeneration. *Stem Cells,* 33**,** 2456-68.

572 KANEHISA, M., SATO, Y., KAWASHIMA, M., FURUMICHI, M. & TANABE, M. 2016.
573 KEGG as a reference resource for gene and protein annotation. *Nucleic Acids Res,* 44**,** D457-62.

574 KIM, D., KIM, S., PARK, J., CHANG, H. R., CHANG, J., AHN, J., PARK, H., PARK, J., SON,
575 N., KANG, G., KIM, J., KIM, K., PARK, M. S., KIM, Y. K. & BAEK, D. 2021a. A high-resolution
576 temporal atlas of the SARS-CoV-2 translatome and transcriptome. *Nat Commun,* 12**,** 5120.

577 KIM, D., SUNG, Y. M., PARK, J., KIM, S., KIM, J., PARK, J., HA, H., BAE, J. Y., KIM, S. &
578 BAEK, D. 2016. General rules for functional microRNA targeting. *Nat Genet,* 48**,** 1517-1526.

579 KIM, J. H., PARK, I., SHIN, H. R., RHEE, J., SEO, J. Y., JO, Y. W., YOO, K., HANN, S. H.,
580 KANG, J. S., PARK, J., KIM, Y. L., MOON, J. Y., CHOI, M. H. & KONG, Y. Y. 2021b. The
581 hypothalamic-pituitary-gonadal axis controls muscle stem cell senescence through autophagosome
582 clearance. *J Cachexia Sarcopenia Muscle,* 12**,** 177-191.

583 KOLBERG, L., RAUDVERE, U., KUZMIN, I., ADLER, P., VILO, J. & PETERSON, H. 2023.
584 g:Profiler-interoperable web service for functional enrichment analysis and gene identifier
585 mapping (2023 update). *Nucleic Acids Res,* 51**,** W207-W212.

586 LANGMEAD, B. & SALZBERG, S. L. 2012. Fast gapped-read alignment with Bowtie 2. *Nat*
587 *Methods,* 9**,** 357-9.

588 LIU, L., CHARVILLE, G. W., CHEUNG, T. H., YOO, B., SANTOS, P. J., SCHROEDER, M. &
589 RANDO, T. A. 2018. Impaired Notch Signaling Leads to a Decrease in p53 Activity and Mitotic
590 Catastrophe in Aged Muscle Stem Cells. *Cell Stem Cell,* 23**,** 544-556 e4.

591 LIU, L., CHEUNG, T. H., CHARVILLE, G. W., HURGO, B. M., LEAVITT, T., SHIH, J.,
592 BRUNET, A. & RANDO, T. A. 2013. Chromatin modifications as determinants of muscle stem
593 cell quiescence and chronological aging. *Cell Rep,* 4**,** 189-204.

594 LIU, L., CHEUNG, T. H., CHARVILLE, G. W. & RANDO, T. A. 2015. Isolation of skeletal
595 muscle stem cells by fluorescence-activated cell sorting. *Nat Protoc,* 10**,** 1612-24.

596 LOVE, M. I., HUBER, W. & ANDERS, S. 2014. Moderated estimation of fold change and
597 dispersion for RNA-seq data with DESeq2. *Genome Biol,* 15**,** 550.

598 MARTIN, M. 2011. Cutadapt removes adapter sequences from high-throughput sequencing reads.
599 *2011,* 17**,** 3.

600 MJ, S. & AL., E. 2023. Senescence atlas reveals an aged-like inflamed niche that blunts muscle
601 regeneration. *Nature,* 613**,** 169–178.

602 NAGY, E. & MAQUAT, L. E. 1998. A rule for termination-codon position within intron-
603 containing genes: when nonsense affects RNA abundance. *Trends Biochem Sci,* 23**,** 198-9.

604 OPRESCU, S. N., YUE, F., QIU, J., BRITO, L. F. & KUANG, S. 2020. Temporal Dynamics and
605 Heterogeneity of Cell Populations during Skeletal Muscle Regeneration. *iScience,* 23**,** 100993.

606 PALA, F., DI GIROLAMO, D., MELLA, S., YENNEK, S., CHATRE, L., RICCHETTI, M. &
607 TAJBAKHSH, S. 2018. Distinct metabolic states govern skeletal muscle stem cell fates during
608 prenatal and postnatal myogenesis. *J Cell Sci,* 131.

609 PRICE, F. D., VON MALTZAHN, J., BENTZINGER, C. F., DUMONT, N. A., YIN, H., CHANG,
610 N. C., WILSON, D. H., FRENETTE, J. & RUDNICKI, M. A. 2014. Inhibition of JAK-STAT
611 signaling stimulates adult satellite cell function. *Nat Med,* 20**,** 1174-81.

PRUITT, K. D., TATUSOVA, T. & MAGLOTT, D. R. 2007. NCBI reference sequences (RefSeq): a curated non-redundant sequence database of genomes, transcripts and proteins. *Nucleic Acids Res,* 35**,** D61-5.

RELAIX, F., BENCZE, M., BOROK, M. J., DER VARTANIAN, A., GATTAZZO, F., MADEMTZOGLOU, D., PEREZ-DIAZ, S., PROLA, A., REYES-FERNANDEZ, P. C., ROTINI, A. & TAGLIETTI, T. 2021. Perspectives on skeletal muscle stem cells. *Nat Commun,* 12**,** 692.

RISSO, D., NGAI, J., SPEED, T. P. & DUDOIT, S. 2014. Normalization of RNA-seq data using factor analysis of control genes or samples. *Nat Biotechnol,* 32**,** 896-902.

RYGIEL, K., PICARD, M. & TURNBULL, D. 2016. The ageing neuromuscular system and sarcopenia: a mitochondrial perspective. *J Physiol,* 594**,** 4499--4512.

SACCO, A., DOYONNAS, R., KRAFT, P., VITOROVIC, S. & BLAU, H. M. 2008. Self-renewal and expansion of single transplanted muscle stem cells. *Nature,* 456**,** 502-6.

SAITO, Y. & CHIKENJI, T. S. 2021. Diverse Roles of Cellular Senescence in Skeletal Muscle Inflammation, Regeneration, and Therapeutics. *Front Pharmacol,* 12**,** 739510.

SAMBASIVAN, R., YAO, R., KISSENPFENNIG, A., VAN WITTENBERGHE, L., PALDI, A., GAYRAUD-MOREL, B., GUENOU, H., MALISSEN, B., TAJBAKHSH, S. & GALY, A. 2011. Pax7-expressing satellite cells are indispensable for adult skeletal muscle regeneration. *Development,* 138**,** 3647-56.

SCHULER, S. C., KIRKPATRICK, J. M., SCHMIDT, M., SANTINHA, D., KOCH, P., DI SANZO, S., CIRRI, E., HEMBERG, M., ORI, A. & VON MALTZAHN, J. 2021. Extensive remodeling of the extracellular matrix during aging contributes to age-dependent impairments of muscle stem cell functionality. *Cell Rep,* 35**,** 109223.

TANG, H., INOKI, K., BROOKS, S. V., OKAZAWA, H., LEE, M., WANG, J., KIM, M., KENNEDY, C. L., MACPHERSON, P. C. D., JI, X., VAN ROEKEL, S., FRAGA, D. A., WANG, K., ZHU, J., WANG, Y., SHARP, Z. D., MILLER, R. A., RANDO, T. A., GOLDMAN, D., GUAN, K. L. & SHRAGER, J. B. 2019. mTORC1 underlies age-related muscle fiber damage and loss by inducing oxidative stress and catabolism. *Aging Cell,* 18**,** e12943.

WASKOM, M. L. 2021. seaborn: statistical data visualization. *JOSS,* 6**,** 3021.

XU, M., PIRTSKHALAVA, T., FARR, J. N., WEIGAND, B. M., PALMER, A. K., WEIVODA, M. M., INMAN, C. L., OGRODNIK, M. B., HACHFELD, C. M., FRASER, D. G., ONKEN, J. L., JOHNSON, K. O., VERZOSA, G. C., LANGHI, L. G. P., WEIGL, M., GIORGADZE, N., LEBRASSEUR, N. K., MILLER, J. D., JURK, D., SINGH, R. J., ALLISON, D. B., EJIMA, K., HUBBARD, G. B., IKENO, Y., CUBRO, H., GAROVIC, V. D., HOU, X., WEROHA, S. J., ROBBINS, P. D., NIEDERNHOFER, L. J., KHOSLA, S., TCHKONIA, T. & KIRKLAND, J. L. 2018. Senolytics improve physical function and increase lifespan in old age. *Nat Med,* 24**,** 1246-1256.

648 ZHANG, H., RYU, D., WU, Y., GARIANI, K., WANG, X., LUAN, P., D'AMICO, D., ROPELLE,
649 E. R., LUTOLF, M. P., AEBERSOLD, R., SCHOONJANS, K., MENZIES, K. J. & AUWERX, J.
650 2016. NAD(+) repletion improves mitochondrial and stem cell function and enhances life span in
651 mice. *Science,* 352**,** 1436-43.

652

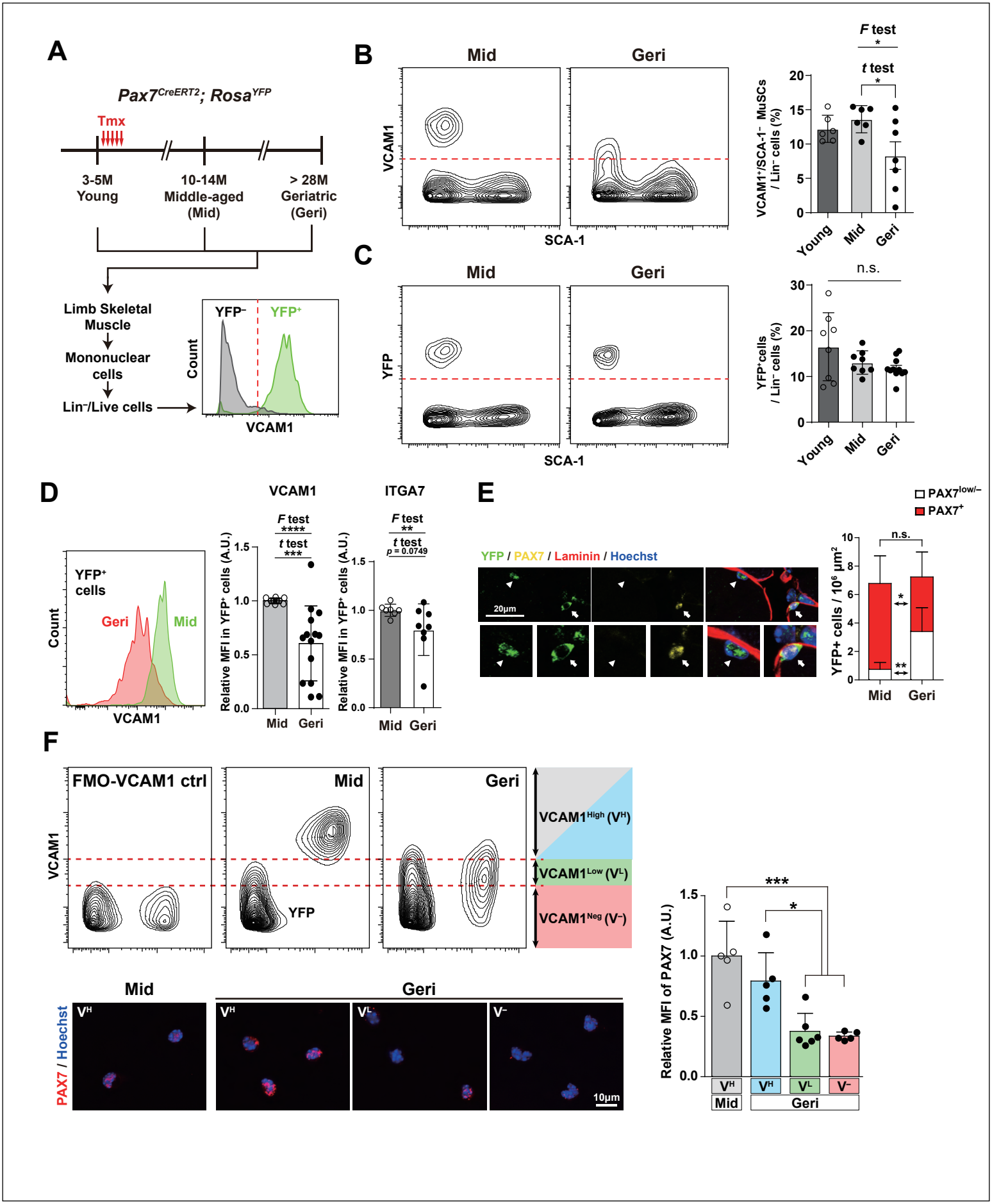
A
Pax7CreERT2; RosaYFP
Tmx
3-5M Young
10-14M Middle-aged (Mid)
> 28M Geriatric (Geri)
Limb Skeletal Muscle
Mononuclear cells
Lin−/Live cells
YFP−
YFP+
Count
VCAM1
B
Mid
Geri
VCAM1
SCA-1
F test
t test
VCAM1+/SCA-1− MuSCs / Lin− cells (%)
Young
Mid
Geri
C
YFP
n.s.
YFP+cells / Lin− cells (%)
D
YFP+ cells
Geri
Mid
VCAM1
ITGA7
Relative MFI in YFP+ cells (A.U.)
p = 0.0749
E
PAX7low/−
PAX7+
YFP / PAX7 / Laminin / Hoechst
20μm
YFP+ cells / 10⁶ μm²
F
FMO-VCAM1 ctrl
YFP
VCAM1High (VH)
VCAM1Low (VL)
VCAM1Neg (V−)
PAX7 / Hoechst
10μm
Relative MFI of PAX7 (A.U.)

653 **Figure. 1. The YFP$^+$ cells from *Pax7^{CreERT2};Rosa^{YFP}* mice do not decrease with age.** (**A**)
654 Scheme of MuSC labeling in *Pax7^{CreERT2};Rosa^{YFP}* mice (MuSC^{YFP}) and analysis at middle (Mid)
655 and geriatric age (Geri) using fluorescence-activated cell sorting (FACS) strategy for isolation of
656 YFP$^+$ MuSCs using traditional marker, VCAM1. (**B, C**) Representative plot and quantification for
657 VCAM1$^+$ MuSCs (**B**) and YFP$^+$ cells (**C**) in lineage negative (Lin$^-$) cells of Young (n=6 and n=8
658 each), Mid (n = 7, n = 8, each) and Geri (n = 6, n = 11, each) MuSC^{YFP}, Welch's *t* test and *F*-test;
659 p = 0.0441 and 0.0460 for (**B**), respectively. (**D**) Representative FACS histogram and
660 quantification of VCAM1 and ITGA7 expression in YFP$^+$ cells of Mid and Geri MuSC^{YFP}.
661 Quantification of relative VCAM1 and ITGA7 mean fluorescence intensity (MFI) in YFP$^+$ cells
662 of Mid (n = 12, n = 6, each) and Geri (n = 14, n = 8, each) MuSC^{YFP}, Welch's *t* test and *F*-test; p
663 = 0.0009 and <0.0001. (**E**) Representative images and quantification of immunohistochemistry
664 staining for Hoechst (Blue), YFP (Green), PAX7 (Yellow), and Laminin (Red) in the *Tibialis*
665 *Anterior* (TA) of MuSC^{YFP}. Arrows indicate PAX7$^+$/YFP$^+$ cells and arrowheads indicate PAX7$^-$
666 /YFP$^+$ cells under basal lamina. Quantification of the number of Pax7$^+$/YFP$^+$ and PAX7$^-$/YFP$^+$
667 cells from IHC staining of TA in Mid (n = 7) and Geri (n = 9) MuSC^{YFP}, two-way ANOVA
668 followed by Bonferroni's multiple comparison test, PAX7$^+$/YFP$^+$; p = 0.0205, PAX7$^-$/YFP$^+$; p =
669 0.0051. (**F**) Division of YFP$^+$ cells according to their VCAM1 MFI as VCAM1^{High} (V^H),
670 VCAM1^{Low} (V^L), and VCAM1^{Neg} (V$^-$) followed by representative images and quantification of
671 immunocytochemistry (ICC) staining for Hoechst (Blue), PAX7 (Red) of YFP$^+$ cells.
672 Quantification of PAX7 fluorescence intensity from isolated YFP$^+$ cells of Mid V^H, Geri V^H, V$^-$
673 (n = 5, each), and V^L (n=6), one-way ANOVA followed by Bonferroni's multiple comparison test;
674 p = 0.0004 (vs Mid V^H), and 0.0179, 0.0123 (Geri V^H vs V^L, V$^-$, respectively).
675

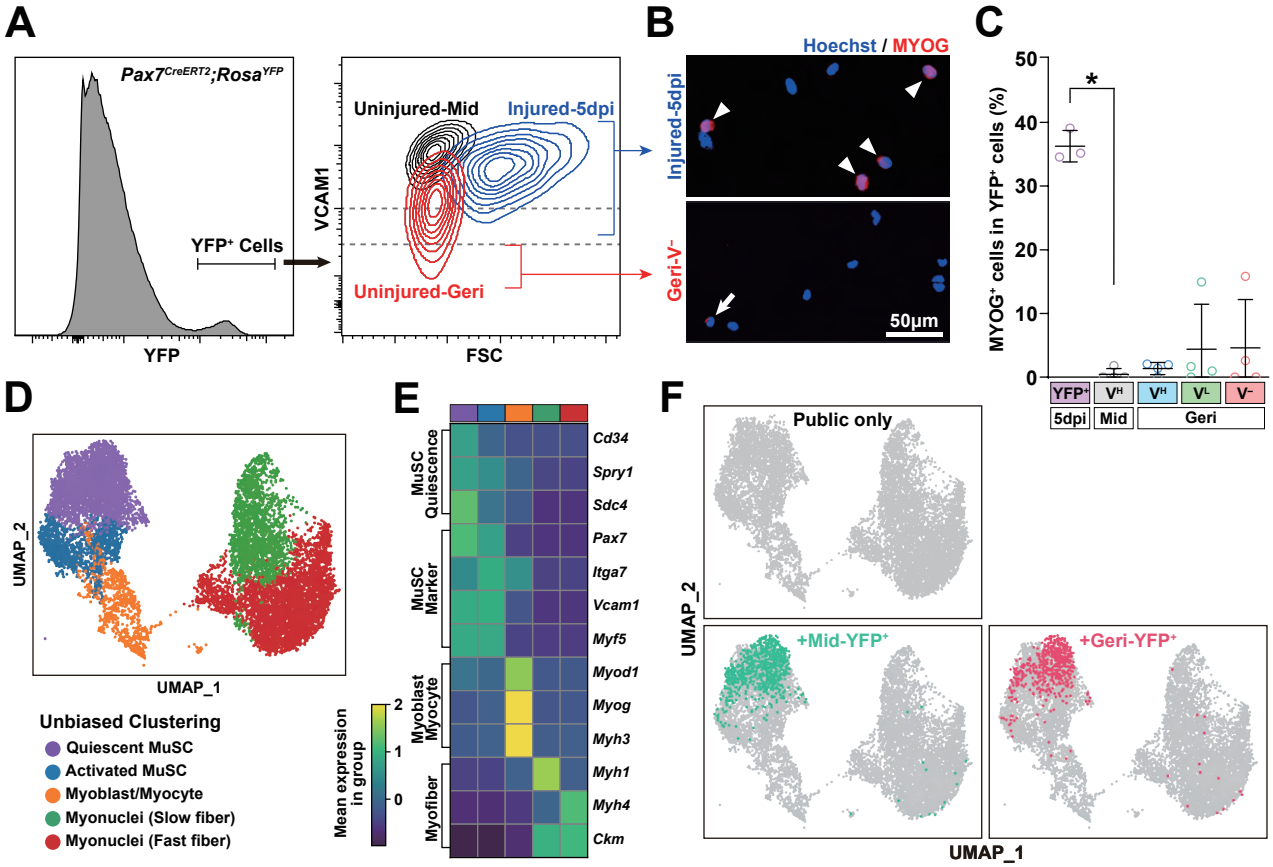
A
Pax7CreERT2;RosaYFP
YFP+ Cells
YFP
VCAM1
FSC
Uninjured-Mid
Injured-5dpi
Uninjured-Geri
B
Hoechst / MYOG
Injured-5dpi
Geri-V-
50µm
C
MYOG+ cells in YFP+ cells (%)
50
40
30
20
10
0
*
YFP+
VH
VH
VL
V-
5dpi
Mid
Geri
D
UMAP_2
UMAP_1
Unbiased Clustering
Quiescent MuSC
Activated MuSC
Myoblast/Myocyte
Myonuclei (Slow fiber)
Myonuclei (Fast fiber)
E
MuSC Quiescence
MuSC Marker
Myoblast Myocyte
Myofiber
Cd34
Spry1
Sdc4
Pax7
Itga7
Vcam1
Myf5
Myod1
Myog
Myh3
Myh1
Myh4
Ckm
Mean expression in group
2
1
0
F
Public only
+Mid-YFP+
+Geri-YFP+
UMAP_2
UMAP_1

676 **Figure 2. YFP$^+$/VCAM1$^-$ cells are quiescent MuSCs.** (**A**) Representative FACS plot for YFP$^+$
677 cells from uninjured Mid and Geri, and injured-5dpi young (20-weeks-old) mice. (**B**, **C**)
678 Representative images (**B**) of ICC staining for Hoechst (Blue) and MYOG (Red), and
679 quantification (**C**) of MYOG$^+$ cells in each YFP$^+$ cell, one-way ANOVA followed by Bonferroni's
680 multiple comparison test; p = 0.0139 between YFP+ cells of injured-5dpi and Mid V^H. (**D**)
681 Uniform manifold approximation and projection (UMAP) plot of YFP$^+$ cells integrated with public
682 scRNA-seq data of MuSC-lineage mononucleated cells in uninjured/injured muscle colored by
683 cell types. (**E**) Matrix plot for representative genes of specific cell types for determining the
684 identities of each cluster. (**F**) The localization of Mid and Geri YFP$^+$ cells in this study on UMAP
685 plot of Fig. 2D.
686

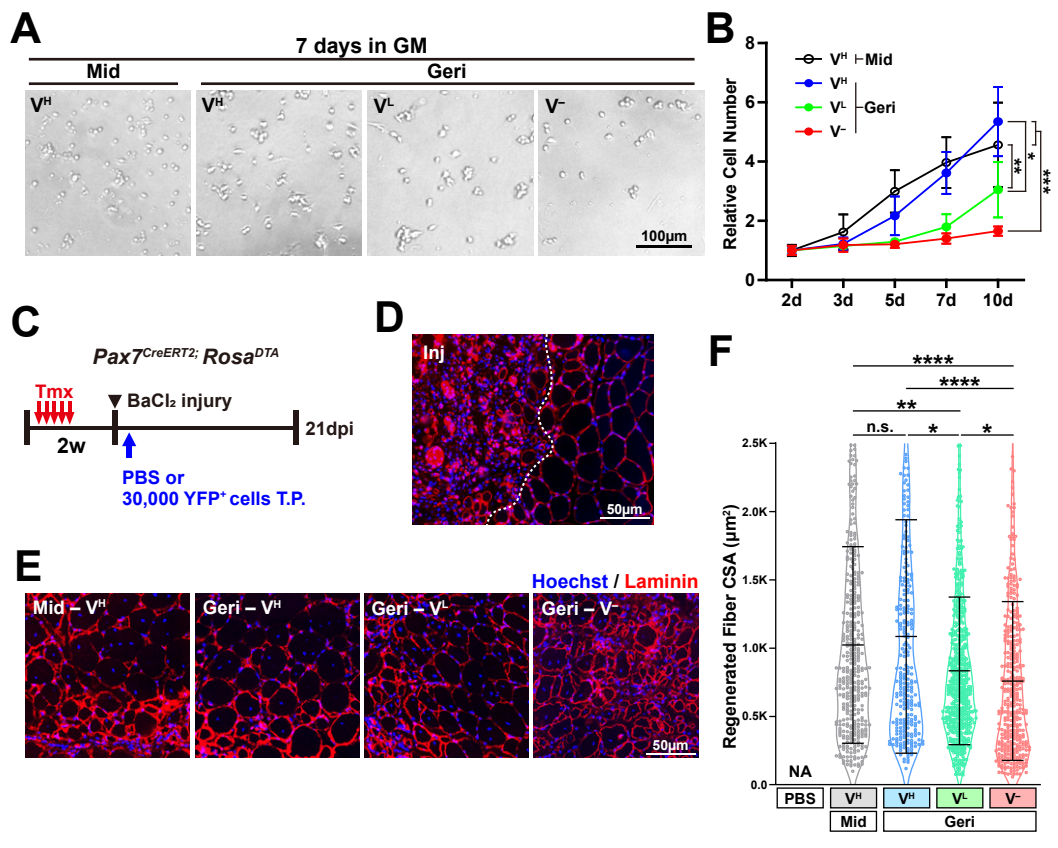
A
7 days in GM
Mid
Geri
V^H
V^H
V^L
V^-
100µm
B
Relative Cell Number
V^H Mid
V^H
V^L
V^-
Geri
2d
3d
5d
7d
10d
C
Pax7^CreERT2; Rosa^DTA
Tmx
BaCl₂ injury
2w
21dpi
PBS or
30,000 YFP⁺ cells T.P.
D
Inj
50µm
E
Hoechst / Laminin
Mid – V^H
Geri – V^H
Geri – V^L
Geri – V^-
50µm
F
Regenerated Fiber CSA (µm²)
n.s.
NA
PBS
V^H
V^H
V^L
V^-
Mid
Geri

687 **Figure 3. Compromised but retained functionality in VCAM1^{-} MuSCs.** (**A**) Representative
688 bright field images of Mid V^H, Geri V^H, V^L, and V^- MuSCs at 7 days culture in MuSC growth
689 media. (**B**) Proliferation measured by relative cell number at 2, 3, 5, 7, and 10 days, two-way
690 ANOVA followed by Bonferroni's multiple comparison test; p = 0.0029 and 0.0002 (Mid V^H vs
691 V^L and V^-, respectively) and p= 0.0102 and 0.0006 (Geri V^H vs VL and V^-, respectively). (**C**)
692 Experimental schematics of transplantation of YFP^+ cells to TA muscle of *Pax7^{CreERT2};Rosa^{DTA}*
693 mice. (**D, E**) Representative images of IHC staining for Hoechst (Blue) and Laminin (Red) in PBS
694 treated TA muscle section following injury. (**D**) Left side of the dotted line show areas affected by
695 BaCl2 injury and right side shows uninjured areas of the muscle. (**E**) IHC staining shows
696 centralized myofibers in all images, with notably smaller myofibers in Geri V^-. (**F**) Quantification
697 of cross sectional area of regenerated fibers from TA muscle of *Pax7^{CreERT2};Rosa^{DTA}* mice
698 transplanted with Mid V^H, Geri V^H, V^L, and V^- at 21 dpi, n = 3 for each group. Total 43 data points
699 are outside of the axis. Kruskal-Wallis test followed by Dunn's multiple comparison test; $p <$
700 0.0001 (Mid and Geri V^H vs V^-) and p = 0.0059 (Mid V^H vs Geri V^L), 0.0149 (Geri V^H vs V^L) and
701 0.0143 (Geri V^L vs V^-).
702

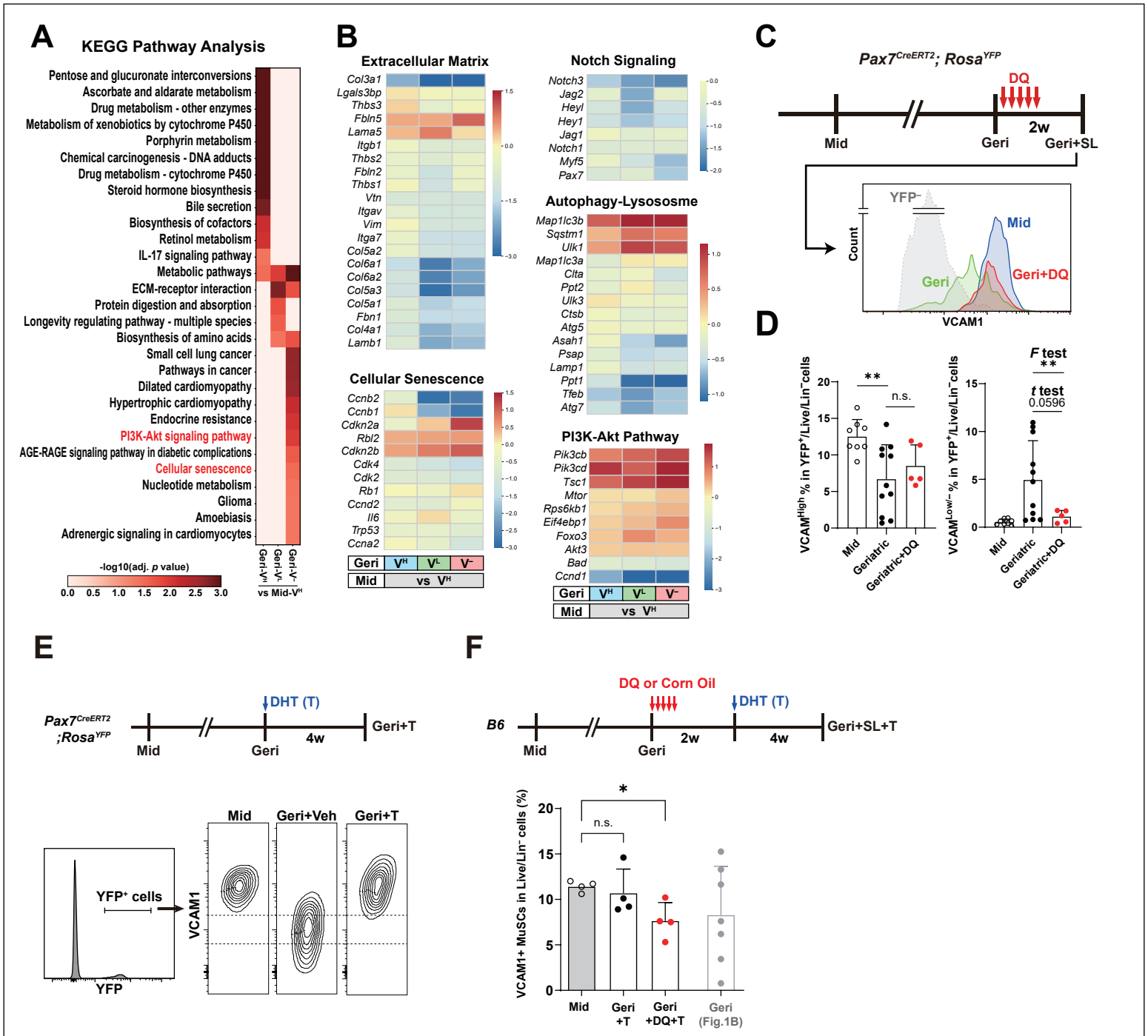
A
KEGG Pathway Analysis
Pentose and glucuronate interconversions
Ascorbate and aldarate metabolism
Drug metabolism - other enzymes
Metabolism of xenobiotics by cytochrome P450
Porphyrin metabolism
Chemical carcinogenesis - DNA adducts
Drug metabolism - cytochrome P450
Steroid hormone biosynthesis
Bile secretion
Biosynthesis of cofactors
Retinol metabolism
IL-17 signaling pathway
Metabolic pathways
ECM-receptor interaction
Protein digestion and absorption
Longevity regulating pathway - multiple species
Biosynthesis of amino acids
Small cell lung cancer
Pathways in cancer
Dilated cardiomyopathy
Hypertrophic cardiomyopathy
Endocrine resistance
PI3K-Akt signaling pathway
AGE-RAGE signaling pathway in diabetic complications
Cellular senescence
Nucleotide metabolism
Glioma
Amoebiasis
Adrenergic signaling in cardiomyocytes
-log10(adj. p value)
0.0 0.5 1.0 1.5 2.0 2.5 3.0
Geri-VH
Geri-VL
Geri-V-
vs Mid-VH
B
Extracellular Matrix
Col3a1
Lgals3bp
Thbs3
Fbln5
Lama5
Itgb1
Thbs2
Fbln2
Thbs1
Vtn
Itgav
Vim
Itga7
Col5a2
Col6a1
Col6a2
Col5a3
Col5a1
Fbn1
Col4a1
Lamb1
Cellular Senescence
Ccnb2
Ccnb1
Cdkn2a
Rbl2
Cdkn2b
Cdk4
Cdk2
Rb1
Ccnd2
Il6
Trp53
Ccna2
Geri VH VL V-
Mid vs VH
Notch Signaling
Notch3
Jag2
Heyl
Hey1
Jag1
Notch1
Myf5
Pax7
Autophagy-Lysosome
Map1lc3b
Sqstm1
Ulk1
Map1lc3a
Clta
Ppt2
Ulk3
Ctsb
Atg5
Asah1
Psap
Lamp1
Ppt1
Tfeb
Atg7
PI3K-Akt Pathway
Pik3cb
Pik3cd
Tsc1
Mtor
Rps6kb1
Eif4ebp1
Foxo3
Akt3
Bad
Ccnd1
Geri VH VL V-
Mid vs VH
C
Pax7CreERT2; RosaYFP
DQ
2w
Mid
Geri
Geri+SL
YFP-
Mid
Geri
Geri+DQ
Count
VCAM1
D
VCAMHigh % in YFP+/Live/Lin-cells
**
n.s.
Mid
Geriatric
Geriatric+DQ
VCAMLow/- % in YFP+/Live/Lin-cells
F test
**
t test
0.0596
Mid
Geriatric
Geriatric+DQ
E
Pax7CreERT2 ;RosaYFP
DHT (T)
Mid
Geri
4w
Geri+T
YFP+ cells
YFP
VCAM1
Mid
Geri+Veh
Geri+T
F
B6
DQ or Corn Oil
DHT (T)
Mid
Geri
2w
4w
Geri+SL+T
VCAM1+ MuSCs in Live/Lin- cells (%)
*
n.s.
Mid
Geri +T
Geri +DQ+T
Geri (Fig.1B)

703 **Figure 4. Senescence characteristics of VCAM1^{-}/YFP^{+} cells and their rejuvenation by DHT**
704 **supplementation.** (**A**) The statistical significance of Kyoto-Encyclopedia of Genes and Genomes
705 (KEGG) pathways, associated with differentially expressed genes (DEGs) between Mid V^{H} and
706 Geri V^{H}, V^{L} and V^{-}, visualized as a heatmap. (**B**) Heatmap of relative expressions of representative
707 genes known to be altered in aged MuSCs compared to Mid V^{H}. (**C**) Experimental schematics of
708 senolytics, dasatinib and quercetin (DQ), treatment in MuSC^{YFP} at geriatric age and representative
709 FACS histogram of VCAM1 expression Mid, Geri, and Geri treated with SL (Geri+DQ) mice. (**D**)
710 Quantification of the percentage of VCAM1^{High} and VCAM1$^{Low/-}$cells divided by VCAM1
711 expression levels in Mid (n = 8) and Geri mice with (n = 5) or without (n = 11) senolytics, 2 tailed
712 student's t test, p = 0.0051 for Mid vs Geri in VCAM1^{High} and F test: p = 0.0026 for Geriatric vs
713 Geriatric+DQ in VCAM1$^{Low/-}$. (**E**) Experimental schematics of dihydrotestosterone (DHT)
714 treatment and FACS plot of VCAM1 expression levels for YFP^{+} cells in MuSC^{YFP}. (**F**)
715 Experimental schematics of DQ and DHT treatment and quantification of the percentage of
716 VCAM1^{High} MuSCs in Live/Lin– cells in Mid and Geri B6 mice (n = 4 in each), 2 tailed student's
717 t test, p = 0.0113 for Young vs Geri+DQ+T.
718

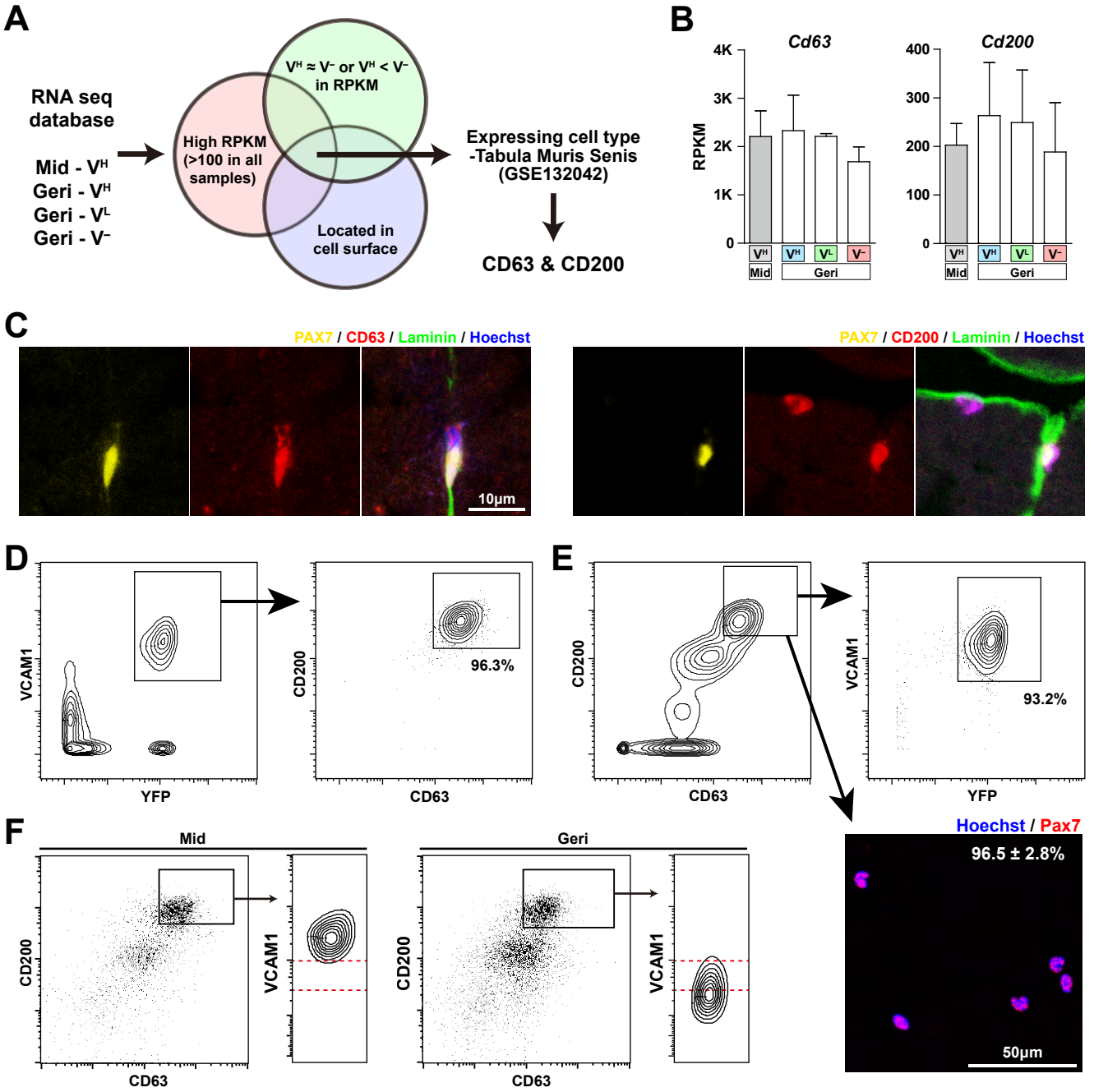
A
RNA seq database
Mid - VH
Geri - VH
Geri - VL
Geri - V−
High RPKM (>100 in all samples)
VH ≈ V− or VH < V− in RPKM
Located in cell surface
Expressing cell type -Tabula Muris Senis (GSE132042)
CD63 & CD200
B
Cd63
Cd200
RPKM
4K
3K
2K
1K
0
400
300
200
100
0
VH
VH
VL
V−
Mid
Geri
C
PAX7 / CD63 / Laminin / Hoechst
PAX7 / CD200 / Laminin / Hoechst
10μm
D
VCAM1
YFP
CD200
CD63
96.3%
E
CD200
CD63
VCAM1
YFP
93.2%
F
Mid
Geri
CD200
CD63
VCAM1
Hoechst / Pax7
96.5 ± 2.8%
50μm

719 **Figure 5. Detection of GERI-MuSCs using CD63/CD200-based FACS strategy.** (**A**) Vann
720 Diagram schematics showing criteria used to select MuSC marker candidate CD63 and CD200,
721 from RNA seq database. (**B**) Relative gene expressions of *Cd63* and *Cd200* shown in RPKMs from
722 Mid V^H, Geri V^H, V^L, and V^- MuSCs. (**C**, **D**) Representative IHC staining images for Hoechst
723 (Blue), Laminin (Green), PAX7 (Yellow) with CD63 (red, **C**) or CD200 (red, **D**) in the TA muscle
724 of Mid $MuSC^{YFP}$. (**E**) Representative FACS plot from young mice showing 96.3% of
725 $VCAM1^+/YFP^+$ cells are $CD63^{high}/CD200^{high}$. (**F**) Representative FACS plot from young mice
726 showing 93.2% of $CD63^{high}/CD200^{high}$ cells are $VCAM1^+/YFP^+$, and ICC staining of this
727 population shows that 96.5±2.8% are $PAX7^+$. (**G**) Representative FACS plot of MuSCs of *B6* Mid
728 and Geri mice gated by CD63 and CD200 and their VCAM1 expression level.
729

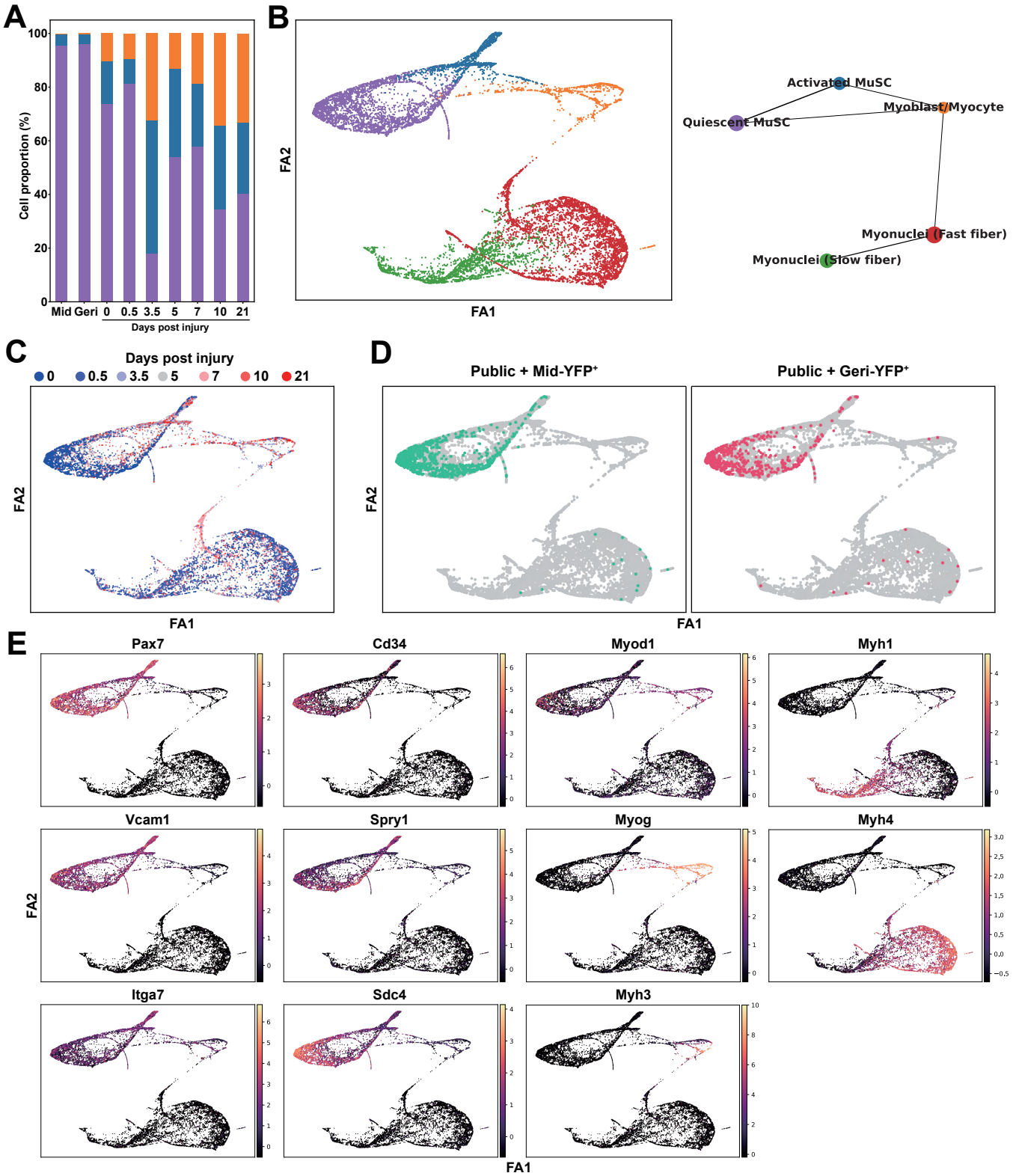
A
Cell proportion (%)
Mid Geri 0 0.5 3.5 5 7 10 21
Days post injury
B
FA2
FA1
Activated MuSC
Quiescent MuSC
Myoblast/Myocyte
Myonuclei (Fast fiber)
Myonuclei (Slow fiber)
C
Days post injury
0 0.5 3.5 5 7 10 21
FA2
FA1
D
Public + Mid-YFP+
Public + Geri-YFP+
FA2
FA1
E
Pax7
Cd34
Myod1
Myh1
Vcam1
Spry1
Myog
Myh4
Itga7
Sdc4
Myh3
FA2
FA1

730 **Fig. S1. Quiescent MuSC characteristics of YFP$^+$ cells.** (**A**) Stacked bar graph of myogenic cell
731 cluster proportion determined in Fig. 2.at Mid, Geri, and each days-post-injury (DPI) of public
732 data. (**B**) Force-directed graph (left) and partition-based graph abstraction (PAGA) connectivities
733 (right) of YFP$^+$ cells integrated with public scRNA-seq data described in Fig. 2, colored by cell
734 types. (**C**) Force-directed graph showing identities of cells based on the days-post-injury. (**D**)
735 Force-directed graph showing the locations of YFP$^+$ cells of Mid and Geri in this study. (**E**) The
736 expression levels of representative genes of specific cell types shown in the force-directed graph.
737

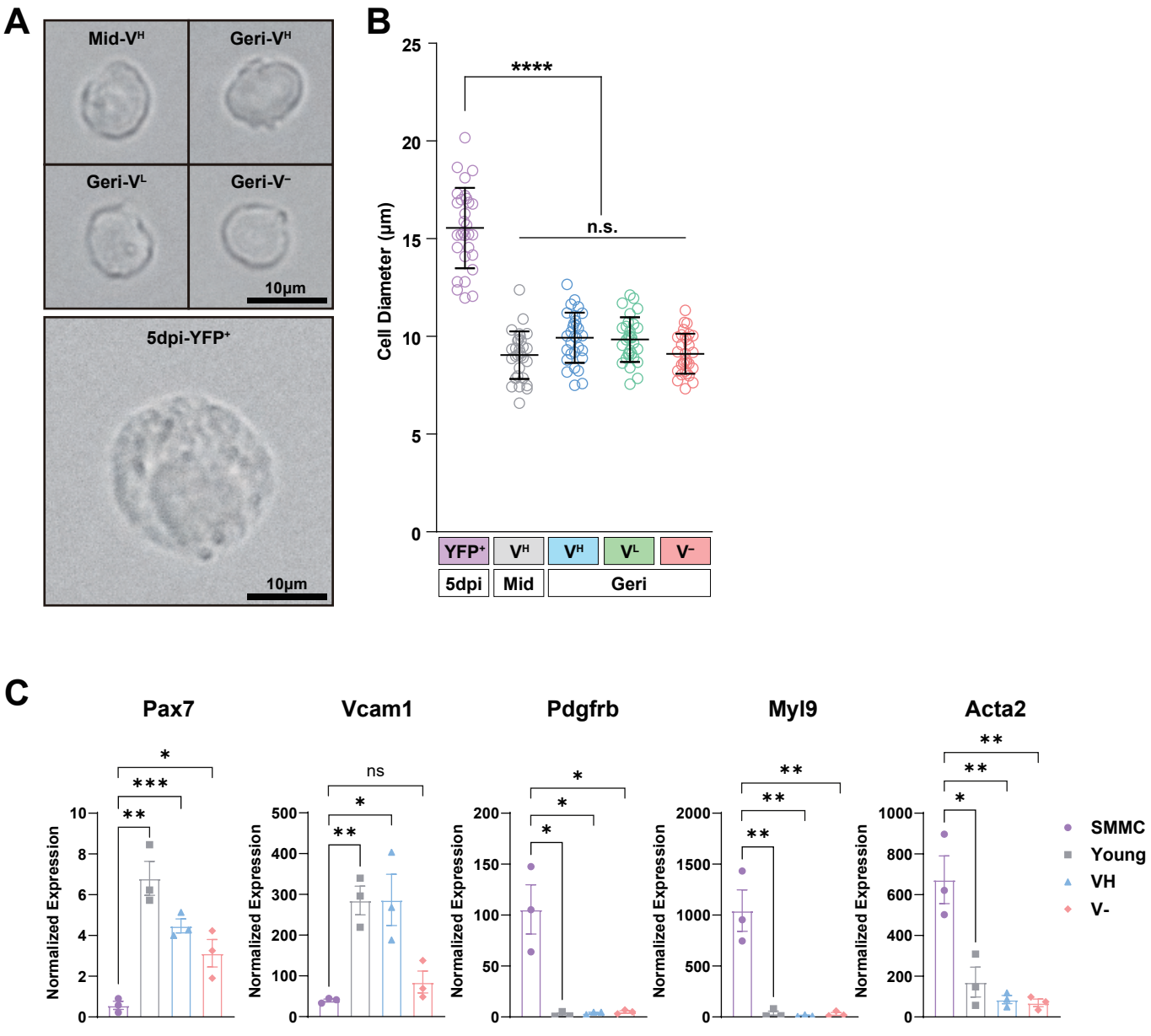
A
Mid-V^H
Geri-V^H
Geri-V^L
Geri-V^-
10μm
5dpi-YFP^+
10μm
B
Cell Diameter (μm)
****
n.s.
YFP^+
V^H
V^H
V^L
V^-
5dpi
Mid
Geri
C
Pax7
Vcam1
Pdgfrb
Myl9
Acta2
Normalized Expression
ns
SMMC
Young
VH
V-

738 **Fig. S2. VCAM1^{-} cells resemble quiescent MuSCs in size and differ from SMMCs.** (**A**)
739 Representative bright field image of freshly isolated YFP^{+} cells of injured-5dpi young (20-weeks-
740 old), Mid V^{H}, Geri V^{H}, V^{L}, and V^{-}. (**B**) Quantification of cell diameter in YFP^{+} cells of injured-
741 5dpi, Mid V^{H}, Geri V^{H}, V^{L}, and V^{-}, one-way ANOVA followed by Bonferroni's multiple
742 comparison test; p <0.0001 for injured-5dpi vs all YFP^{+} cell groups of uninjured muscle. (**C**)
743 Normalized expression of MuSC marker genes, Pax7 and Vcam1, and smooth muscle
744 mesenchymal cells marker genes, Pdgfrb, Myl9 and Acta2.
745

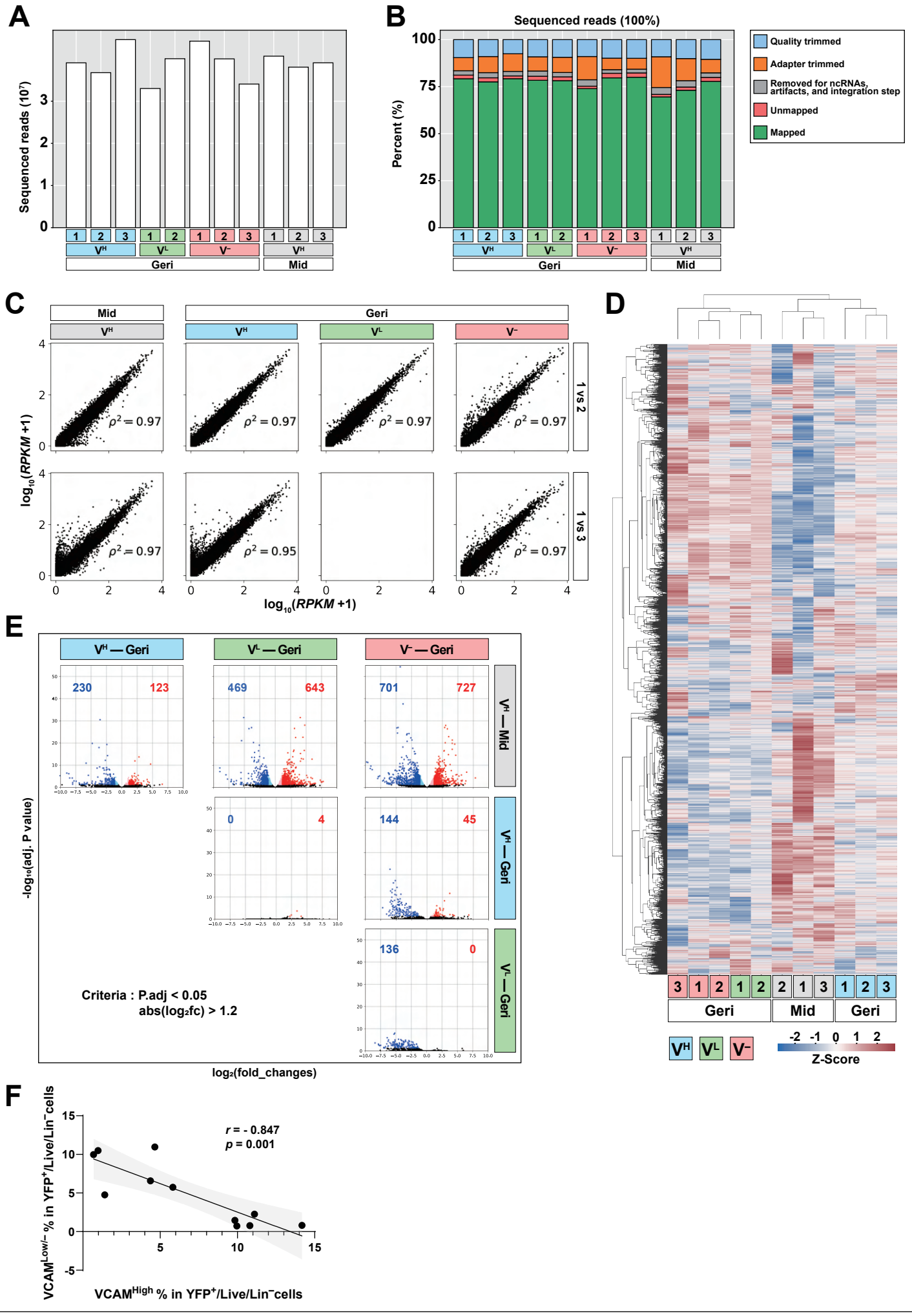
A
Sequenced reads (10^7)
0
1
2
3
1 2 3 1 2 1 2 3 1 2 3
V^H V^L V^- V^H
Geri
Mid
B
Sequenced reads (100%)
Percent (%)
100
75
50
25
0
Quality trimmed
Adapter trimmed
Removed for ncRNAs, artifacts, and integration step
Unmapped
Mapped
C
Mid
Geri
V^H
V^L
V^-
1 vs 2
1 vs 3
$\rho^2 = 0.97$
$\rho^2 = 0.95$
$\log_{10}(RPKM+1)$
D
3 1 2 1 2 2 1 3 1 2 3
Geri
Mid
Geri
Z-Score
-2 -1 0 1 2
E
V^H — Geri
V^L — Geri
V^- — Geri
V^H — Mid
V^H — Geri
V^L — Geri
230 123
469 643
701 727
0 4
144 45
136 0
Criteria : P.adj < 0.05
abs($\log_2$fc) > 1.2
$-\log_{10}$(adj. P value)
$\log_2$(fold_changes)
F
r = - 0.847
p = 0.001
$VCAM^{Low/-}$ % in YFP^+/Live/Lin^-cells
$VCAM^{High}$ % in YFP^+/Live/Lin^-cells

746 **Fig. S3. Validation and basic analysis of transcriptomic data of YFP$^+$ cells.** (**A**) Total number
747 of sequenced reads of each sample. (**B**) The percentage of trimmed reads of each sample for quality
748 control. (**C**) Dot plots of gene expression showing linear correlations of between samples of the
749 same group. The number in the plot represents Spearman Coefficient. (**D**) Hierarchical clustering
750 of bulk RNA-seq samples with gene expression profiles, showing sample similarity (x-axis) and
751 gene similarity (y-axis), illustrating inter-group similarity and similarity between V^H of Mid and
752 Geri and between V^L and V^- of Geri. (**E**) Volcano plots showing differentially expressed genes
753 (DEGs) between groups at a threshold of LFC > 1.2 and adjusted p value < 0.05. The numbers in
754 the plot represent the number of up-regulated (red) and down-regulated (blue) genes compared to
755 the sample indicated in the right of the panel. (**F**) Correlation analysis between the percentages of
756 VCAM1^{High} and VCAM1$^{Low/-}$ cells within YFP$^+$/Live/Lin$^-$ MuSCs isolated from geriatric mice.
757 Each dot represents an individual mouse. A significant negative correlation was observed
758 (Pearson's $r = -0.847$, $p = 0.001$), indicating that a higher proportion of VCAM1^{High} MuSCs is
759 associated with a lower proportion of VCAM1$^{Low/-}$ MuSCs. Shaded area represents the 95%
760 confidence interval of the linear regression.
761

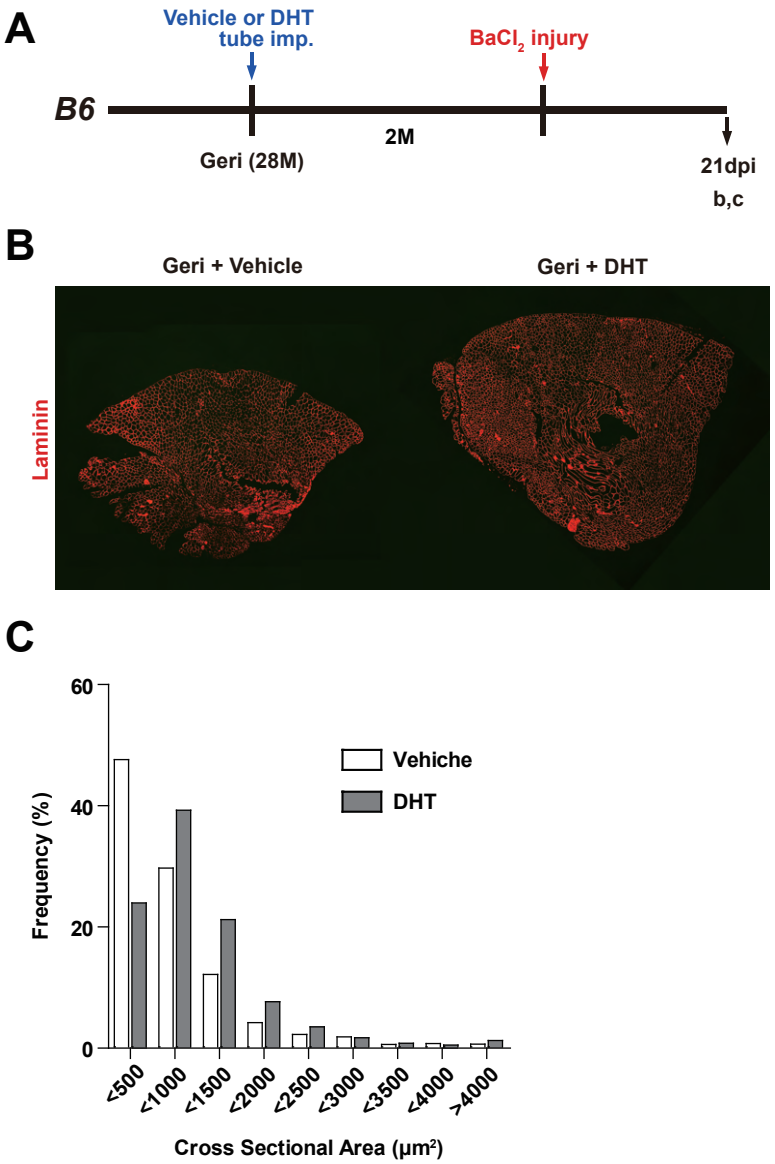
A
Vehicle or DHT
tube imp.
BaCl2 injury
B6
2M
Geri (28M)
21dpi
b,c
B
Geri + Vehicle
Geri + DHT
Laminin
C
60
40
20
0
Frequency (%)
Vehiche
DHT
<500
<1000
<1500
<2000
<2500
<3000
<3500
<4000
>4000
Cross Sectional Area (μm2)

762 **Fig. S4. Rehabilitation of myofiber regeneration capacity in geriatric mice after DHT**
763 **supplementation.**
764 (**A**) Experimental schematics geriatric B6 mice with DHT or vehicle tube implantation before
765 BaCl2 injury. (**B**) Representative images of immunohistochemistry staining for laminin in geriatric
766 mice with vehicle or DHT tube implantation. (**C**) Quantification of the cross-sectional area of the
767 21 dpi TA muscle of geriatric mice after vehicle or DHT tube implantation.
768
769